Report No. 128

March, 1960.

THE COLLEGE OF AERONAUTICS

CRANFIELD

Pressure and Boundary Layer Measurements on a Tapered Swept Wing in Flight

- by -

D. Hyde, M.Sc.(Eng.), D.I.C., A.C.G.I.

(Prepared under Ministry of Aviation Contract No. 6/Aircraft/14002/C.B.6(c).)

SUMMARY

Pressure and boundary layer measurements were made in flight on a full scale swept half-wing mounted as a dorsal fin on the mid fuselage of an Avro Lancaster aircraft. A Reynolds Number range of 0.88×10^6 to 1.86×10^6 per foot was available. The tapered wing had a semi-span of 102.5 ins. and an aspect ratio of 2.87; the quarter chord sweep was 40° and the symmetrical section was RAE 102, of 8% thickness/chord ratio along wind.

Comprehensive static pressure measurements were recorded over a nominal incidence range of 0° to 10°. At mid semi-span and zero incidence, the measured chordwise pressure distribution compared well with theory. The non-dimensional chordwise and spanwise loadings were in close agreement with Kuchemann's predictions, but the experimental lift curve slope was 6% greater than the theoretical value.

From the boundary layer results the positions of the transition fronts were deduced. No laminar flow was obtained on either surface at the highest Reynolds number of 1.86×10^6 per foot, or at incidences of 6° and greater at all test Reynolds numbers.

The secondary flow Reynolds number corresponding to the onset of sweep instability was found to be in the range $80 < N < 133$; Owen's predicted critical value is 125.

LIST OF CONTENTS

LIST OF SYMBOLS

x, y, z	Rectangular co-ordinates; x-axis in direction of main flow, y-axis spanwise, z-axis upwards, origin at leading edge.
c	Local wing chord
$\bar{c}$	Mean wing chord
b	Span
η	$= \frac{2y}{b}$. Non-dimensional spanwise position
ϕ	Angle of sweep
α	Geometric angle of incidence
V_o	Velocity of undisturbed stream
p	Local static pressure
p_o	Free stream static pressure
ρ	Air density
C_p	$= \frac{p - p_o}{\frac{1}{2}\rho V_o^2}$. Pressure coefficient
ΔC_p	Difference of pressure coefficients on upper and lower surface
C_L	Local lift coefficient
$\bar{C}_L$	Total lift coefficient
R_e	Reynolds number
x	Secondary flow Reynolds number
h	x-coordinate of local aerodynamic centre

1. Introduction

The work described in this report constitutes a continuation of the programme of flight testing on swept wings which is being carried out in the Department of Flight at the College of Aeronautics. Experiments on a 45° swept back wing of elliptical cross-section have been made by Burrows (Ref. 1). These were followed by some check tests, using a V-section trailing edge fitted to the same wing (Ref. 2), with the object of verifying that the conclusions of Burrows work would still be applicable to wings of conventional section. However, these checks were of limited extent and, consequently, the present programme was established.

The test aerofoil employed was a Folland Midge production wing of aspect ratio 2.87, mounted, as in the previous tests, as a dorsal fin on the mid-fuselage of an Avro Lancaster Mark 7 aircraft. A boundary layer fence was located 17.5 ins. above the fuselage top skin. This fence helped to isolate the test section from the effects of the fuselage boundary layer and the wake generated along the top of the fuselage by the aircraft's cockpit.

The test programme was restricted to a comprehensive investigation of the static pressure distribution on the wing, over a nominal incidence range of 0° to 10°, and to qualitative boundary layer measurements. To obtain the boundary layer data, a two dimensional technique using fixed combs attached to the aerofoil surface was employed.

The aerodynamic loads on the wing were also to have been measured using an A.C. strain gauge system, but the method was abandoned due to difficulties arising from the imperfect adhesion of the gauges to the beryllium copper surfaces of the loading links attached to the spar post extension.

Flight tests were started in March 1959 and completed by the following June, a total of $14\frac{1}{2}$ hours being flown. The static pressure measurements were completed in 4 flying hours and the boundary layer tests in $6\frac{1}{2}$ hours; calibration work and equipment faults accounted for the remaining time.

2. Experimental Equipment and Technique

2.1. The Aircraft

The test vehicle was the Lancaster Mk. 7, PA 474, used in the previous series of flight tests (Refs. 1 and 2).

2.2. The Test Wing

The only major change in the test wing installation from the previous arrangement was the addition of an electrically operated wing incidence actuator. This was controlled by the pilot for safety reasons, final incidence adjustments being made manually by the observer if necessary.

Limit switches prevented the actuator from over-riding the maximum incidence range of $\pm 10^\circ$.

The test section was a standard Folland Midge half wing, the semi-span being 102.5 ins. measured above the boundary layer fence, the root chord 92.9 ins. at the fence and the projected tip chord 50.0 ins. This gave an aspect ratio of 2.87 for the whole wing. The section along wind was an 8% thick RAE 102, with a quarter chord sweep of 40°. Figure 1 illustrates the geometry of the boundary layer fence in relation to the wing, showing that it is approximately two aerofoil thicknesses wide on each side of the test wing.

Most of the flush pressure plotting holes were fitted without the removal of the wing skin. Each pressure tap consisted of two mating components. The female part was introduced, with the pressure lead attached, from inside the wing and the male part externally through a countersunk location hole in the skin, the two being connected by soft iron wire. Finally, the components were screwed together, the wire was removed to reveal the static pressure hole, and the male part of the connector was made flush with the surrounding skin.

The wing was then prepared, the surface finish being polished black cellulose lacquer. It was noted that, although the section was nominally RAE 102, 'flats' could be detected on the surface corresponding to the front and rear spar datum positions.

2.3. Instrumentation

The manometer, camera installation and sideslip indication system are described in detail in Refs. 1 and 2.

On the 50-tube manometer bank there were two datums, and a U-tube for use in the pressure error correction tests. As the manometer had 46 vacant tubes and 128 pressure plotting holes were available, a 'change-over block' system was incorporated. This system consited of a fixed pressure pad equipped with a quick-release lock which was connected via 46 separate tubes to the manometer; three other interchangeable pads with the same number of protruding tubes on each were coupled to the tappings in the test wing. Thus, up to 46 pressures could be recorded at one instant and the next group quickly registered on the manometer by unlocking and removing the first pad, and then locking into position the second pressure block. A short period ensued when the fluid levels in the manometer stabilised, but the total 'change-over' time was reduced to about five seconds with practice. Both water and carbon tetrachloride were used as manometric fluids, depending on the magnitude of the pressures being measured.

The boundary layer investigation was restricted to an area between 5% and 40% local chord and away from the extreme wing tip. Consequently the two dimensional technique employed previously was used, as the deviation of the streamlines from the freestream direction in this area was small (see for example, Ref. 3). The 13-tube combs and 3-tube "transition indicators" are fully described in Ref. 4.

With a view to using in-flight chemical transition indication methods, a G.S.A.P. 16 mm. cine camera was mounted on top of the port wing tip of the aircraft. Good quality photographic records of the test wing were obtained using a camera speed of 32 frames per second, despite wing tip vibration.

3. The Tests Performed

3.1. Pressure Error Correction

The pressure error correction to the Lancaster's pitot-static system was established using the trailing static method in conjunction with a venturi pitot mounted on a boom protruding from the starboard side of the aircraft's nose. The trailing static was controlled from the door in the rear fuselage, and it remained steady up to a speed of 160 knots. Pressure error correction curves for Lancaster PA 474 are illustrated in Fig. 2.

The pilots A.S.I. was also calibrated in the laboratory and found to have an instrument error of one knot or less over the range of test speeds. When processing the flight test data, the pressure error and instrument error on the A.S.I. were both taken into account.

3.2. Test Wing Zero Incidence Setting

In order to find the aerodynamic zero incidence setting, three pairs of static tubes were positioned at 15% local chord on opposite surfaces of the wing at the spanwise stations B, D and G (see Fig. 1). These were connected to the manometer and the aircraft was flown at various sideslip settings, at each of the three test speeds.

From a plot of the differential pressure in each pair of static tubes against the sideslip indicator reading, the aerodynamic "zero" incidence setting was read off as that corresponding to zero differential pressure. The datum was found to be slightly different at each of the three test speeds. However, this technique was apparently inadequate as the $\bar{C}_L$ - α plot (Fig. 8) indicated a no-lift angle of incidence of -0.3°; thus, all incidences are nominal and subject to a correction of $\alpha = -0.3^{\circ}$.

The required datum could be consistently reproduced in flight to within $\pm \frac{1}{4}^{\circ}$ of sideslip, which can be considered as the maximum repeatability error for the wing incidence setting.

3.3. Static Pressure Distribution

The static pressure and boundary layer measurements were carried out at an altitude of 10,000 ft. and speeds of 90, 140 and 190 knots, corresponding to nominal Reynolds numbers of 0.88, 1.37 and 1.86×10^6 per foot (altimeter pressure error and non-standard temperature corrections not applied).

As the bores of the pressure tubes were easily blocked by water, cloud flying, or even passing through cloud on the climb, was strictly avoided. This particularly applied to the tests described in section 3.4, owing to the extremely small diameter of the boundary layer combs.

Comprehensive static pressure distributions on the wing were recorded over an incidence range of 0° to 10°, in 2° increments. Eight spanwise stations were available, with sixteen chordwise pressure tappings at each station. The tappings were all located on one surface, lower surface distributions being obtained by using the appropriate negative incidence.

3.4. Boundary Layer Measurements

Using three 13-tube combs and four 3-tube combs, alternately spaced, boundary layer measurements were recorded at seven spanwise stations (Fig. 10). Five flights were made with the combs located along 40%, 30%, 20%, 10% and 5% local chord lines.

On the first flight the combs were positioned at 40% local chord, and on subsequent flights they were moved progressively nearer the leading edge. This obviated the possibility of the surface finish deteriorating forward of the combs, due to the repeated removal of the sellotape fixing straps when repositioning the combs and pressure leads after each flight. The wing was cleaned and polished with a chamois leather and soft cloth just prior to each test.

4. The Reduction of Results

4.1. Method

In previous work of a similar nature (Refs. 1, 2), the analysis of the flight test data was a long and tedious task. The tendency for unprocessed experimental records to accumulate was alleviated in the present tests by the use of a Benson-Lehner Oscar E data reduction system.

The manometer film records were projected on to the screen of the Oscar E and, after the scales had been suitably set, pressure coefficients were calculated directly and typed out by a coupled I.B.M. electric typewriter. For conversion of the information from pressure coefficient form to force coefficients, it was reconverted into a punched data tape for input to a Ferranti 'Mercury' digital computer. However, it should be noted that this additional process was only necessary because no punching facility was linked to the Benson-Lehner decimal converter at the time the experiments were conducted; thus, the readout process of the film records on the Benson-Lehner equipment could produce a punched tape output immediately available for input into a high speed digital computer.

To obtain a list of pressure coefficient values in tabulated form from the basic film record of the 50-tube manometer took approximately five minutes, including the time taken in setting the appropriate scales. In addition to a saving in time, this data reduction process also minimised the possibility of mistakes in read-out and calculation.

4.2. Errors

The 'internal' error in the Benson-Lehner system resulted in a maximum error in pressure coefficient of .001. In addition, an error arose due to the imperfect alignment on the projection screen of the cursor line with the manometric fluid level. This optical error could be limited to ± .003 inches, as the definition on the film records was good, the resultant error in C_p being dependent on the magnification of the film and the absolute value of C_p. However, the screen on Oscar E was large (12 inches by 25 inches), and this was used to full advantage when projecting the film records.

Consequently, it is thought that errors due to manometer vibrations and response, together with slight instabilities in the test conditions, predominated over those due to the read-out of the film records, and that the maximum overall error was of the order of ± 0.05 inches of manometric fluid.

5. Discussion of results and Comparisons with Theory

5.1. Static Pressure Measurements

5.1.1. Chordwise pressure distribution and loading

No definite trend with Reynolds number could be established from the pressure distribution curves; as the shift of the curves at different Reynolds numbers for a given incidence and spanwise station was very small, and as the chordwise loading curves under these conditions were virtually identical, it was considered in order to use the average values of pressure coefficient over the test Reynolds number range (see Fig. 3).

The flow conditions existing near mid semi-span on a swept back wing of finite aspect ratio are similar to those on a sheared wing of infinite span, provided that the aspect ratio is not extremely small. As the aspect ratio of the test wing was 2.87 it was considered that root and tip effects at mid semi-span would still be negligible, and that the experimental chordwise pressure distribution at the mid semi-span station could be compared with that predicted by Weber's method (Ref. 5). The distribution was also calculated using the Goldstein Approximation III (Refs. 6, 7) as a further check.

From Fig. 4 it is evident that the theoretical results are in good agreement with the experimental values at zero incidence, the latter being slightly more negative around the mid-chord region. Recent tunnel tests and calculations have indicated that the static pressure field above the mid-upper fuselage of the Lancaster to be virtually ambient; the results on the characteristics of the flow field in this vicinity, quoted in Ref. 8, are subject to an interference correction caused by the substantial nature of the pressure plotting mast. Thus, it would appear that the localised deviation of the pressure distribution from the theoretical prediction was due to slight profile differences of the test wing from a true RAE 102 section and to small local perturbations of pressure in the field. The appearance of 'flats' on the wing surface, as noted in section 2.2, also indicated small profile inaccuracies.

The development of the chordwise pressure distribution with incidence was normal (Fig. 3). There was evidence of separation at the higher incidences near the tip, and the resultant increase of lift at the rear of these sections can be seen in Fig. 8, which illustrates the distribution of local lift.

No tendency for a forward movement of the peak pressure near the tip could be detected. This effect, which is undesirable at high speeds, was presumably obviated by the curved leading edge near the tip, which substantially straightened the isobars in that region (Ref. 9).

The non-dimensional chordwise loadings are plotted in Fig. 5, which indicates close agreement, at the mid semi-span station, between the experimental results and theoretical values based on Kuchemann's technique (Ref. 10).

5.1.2. Spanwise loading

The spanwise distribution of local lift coefficient throughout the incidence range investigated is shown in Fig. 6. After gradually increasing from the value at the centre-section, C_L reached a maximum between the non-dimensional spanwise positions $\eta = 0.6$ and $\eta = 0.7$ and then decreased; however, an increase in C_L near the tip, due to the formation of the tip-vortex, became prominent at an incidence of 8°.

The spanwise load distribution was calculated using Kuchemann's method (Ref. 10), which gives the lift at small incidences only as it is based on linear theory. By treating the tip-vortex as an effective endplate (Ref. 11), the influence of this vortex, which is responsible for the non-linear effects, was estimated. According to W. Mangler, the height of the tip-vortex is given by

$$\frac{h}{b} = \frac{\alpha}{2} \cdot \frac{c_t}{\bar{c}} \cdot \frac{1}{A}$$

where c_t is the tip chord (in the present calculations the projected tip chord was used).

Together with the experimental values, the theoretical spanwise loadings are plotted in Fig. 7. The non-dimensional plot exhibits very close agreement between experiment and theory, the experimental loading being very slightly less at the centre and slightly greater at the tip than the theory predicts. These slight discrepancies were reduced when the tip-vortex effect was considered. However, the dimensional loading curve indicated that, in general, the experimental points are greater than the theoretical values. The tip-vortex effect again tended to bring the two curves into closer agreement, but it is almost certain that the difference was not due solely to an underestimation of this effect, as it would have to be approximately three times as strong to make the two loadings identical.

5.1.3. Overall aerodynamic characteristics.

From Fig. 8 the initial overall lift curve slope was found to be 3.14, compared with the value of 2.97 given by Kuchemann's method. The increased magnitude of the experimental span-wise loading (Fig. 7), and the resultant increase in the lift curve slope, could be due to the following effects :

(i) the finite size of the end-plate might not produce complete reflection; the downwash from the image wing would then be reduced, resulting in an increase in lift coefficient on the half wing compared with the complete wing.

(ii) the body effect of the aircraft's fuselage would tend to increase the lift on the wing.

However, these effects would cause an increase in the lift near the centre of the wing, whereas the most significant difference between experiment and theory occurred well away from the centre, as illustrated in Fig. 7. Thus, it is possible that although Kuchemann's method predicts the non-dimensional chordwise and spanwise loadings accurately, the absolute value of the lift curve slope might be less than the experimental value when considering swept aerofoils of small aspect ratio that also have a large taper ratio.

The spanwise variation of the aerodynamic centre position is shown in Fig. 9, from which the measured values of h/c are seen to be in good agreement with theory. There was the usual tendency for the aerodynamic centre to move forwards in going from the centre of the wing to the tip, but a marked backward shift of the experimental positions near the tip was caused by the tip-vortex effect.

5.2. Boundary Layer Measurements

5.2.1. Transition fronts

As the boundary layer readings were obtained by a fixed comb two dimensional method, and as the results exhibited the usual trends - namely thicker boundary layers on the upper surface and a gradual thickening along the trailing edge towards the tip - only the transition data was considered in detail.

The transition fronts were taken to correspond to the end of the transition region, and were deduced from the rate of growth of the boundary layer and the total head rise indicated by the combs when passing from a laminar to a turbulent zone. Where transition was ill-defined by these techniques, shape parameters were calculated and transition taken to correspond to the point where the shape parameter attained a uniform value corresponding to the turbulent state.

The location of the transition fronts at incidence increments of 2° is indicated in Table 8 and Fig. 10. No laminar flow occurred at the highest test Reynolds number of 1.86×10^6 per foot or at incidences of 6° and greater at all speeds. The flow appeared to be most stable at zero incidence, about twice as much laminar flow occurring at $R_e = 0.88 \times 10^6$ per foot as at $R_e = 1.37 \times 10^6$ per foot. On the lower surface the transition fronts moved rapidly towards the leading edge with increasing incidence, especially at the higher Renolds number where transition was forward of 5% local chord at 6° incidence.

On the upper surface the transition front also moves forward with increasing incidence, but, at the higher Reynolds number, this movement is less rapid than on the lower surface. Thus, the formation of a suction peak and the resultant primary instability appear to mask the increase in sweep stability, compared with the zero incidence case, which was predicted by Owen and Randall (Ref. 12) at small values of lift coefficient for an aerofoil of similar section but of 10% thickness/chord ratio.

However, it should be noted that slight 'flats' which could be detected on the wing surface corresponded to the spar positions. The front spar datum was located at 25% local chord and the rear spar datum was well aft of this - hence results where transition occurred aft of 25% local chord should be treated with reserve.

5.2.2. Secondary Reynolds number

From Owen and Randall's calculations (Fig. 5 of Ref. 13), for the test section employed, the secondary flow Reynolds number has a maximum given by :

$$\frac{x_{max}}{R^{\frac{1}{2}}} = 0.035$$

Note that the thickness/chord ratio normal to the leading edge and the half-chord sweep were used for this estimation.

Let

$$\frac{x_{max}}{R^{\frac{1}{2}}} = \frac{N}{R_{crit}^{\frac{1}{2}}} = 0.035$$

where R_{crit} is the maximum Reynolds number for which the boundary layer near the leading edge is stable. As the secondary flow instability precedes transition, an upper limit on N may be placed as no laminar flow occurred at the test R_e of 1.86×10^6 per foot. Thus, by substitution in the above equation, $N < 133$. Also by considering the maximum extent of laminar flow at zero incidence and the lowest Reynolds number, the less rigorous condition that $N > 80$ may be deduced by assuming that secondary flow instability has not yet occurred under these circumstances.

Hence, $$80 < N < 133$$

Owen's criterion for the onset of secondary flow instability is x approximately equal to 125, which is in the range estimated above by a small margin.

6. Conclusions

Comprehensive static pressure measurments on a full scale swept and tapered wing were recorded over a nominal incidence range of 0° to 10°, at Reynolds numbers between 0.88×10^6 and 1.86×10^6 per foot. At mid semi-span and zero incidence, the measured chordwise pressure distribution compared favourably with that given by Weber's method (Ref. 5) and also the third Goldstein approximation (Ref. 6).

The non-dimensional chordwise and spanwise loadings were in close agreement with Kuchemann's predictions, but the experimental lift curve slope was 6% greater than the theoretical value.

At incidence of 6° and above, separation near the wing tip, with the resultant local lift increase, manifested itself in the pressure distribution curves and caused a rearward shift of the local aerodynamic centre position,

Boundary layer measurements were recorded at 2° incidence increments and indicated that no laminar flow existed on either surface at a Reynolds number of 1.86×10^6 per foot, or at incidences of 6° and greater under all test conditions. At 0° incidence the flow appeared to be most stable, and, in all cases, more laminar flow occurred at an R_e of 0.88×10^6 than at 1.37×10^6 per foot. The forward movement of transition with increasing incidence was, in general, more rapid on the lower surface than on the upper surface.

The secondary flow Reynolds number corresponding to the onset of sweep instability was found to be in the range $80 < N < 133$; Owen's predicted critical value is 125.

7. Acknowledgements

The test programme was sponsored by a Ministry of Aviation contract, and full co-operation was received from all members of the Department of Flight associated with the project.

The author acknowledges the discussions held with Mr. G. M. Lilley, Deputy Head of the Aerodynamics Department. Dr. S. Kirkby, of the Mathematics Department, gave invaluable assistance during the preparation of the computer programme for the reduction of the test data, and the theoretical computations were performed by Mrs. J. M. Tucker of the Aerodynamics Department.

8. References

1. Burrows, F.M. — A theoretical and experimental study of the boundary layer flow on a 45° swept back wing. C. of A. Report No. 109, 1956

2. Walton, J. — Addendum to a theoretical and experimental study of the boundary layer flow on a 45° swept back wing. C. of A. Report No. 109, Addendum 1957.

3. Emslie, K., Hosking, L., Marshall, W.S.D. — Some experiments on the flow in the boundary layer of a 45° swept back untapered wing of aspect ratio 4. C. of A. Report No. 69, Feb.1953.

4. Burrows, F.M. — Equipment used for boundary layer measurements in flight. C. of A. Note No. 49, 1956.

5. Weber, J. — The calculation of the pressure distribution over the surface of two-dimensional and swept wings with symmetrical aerofoil sections. R. & M. 2918, 1956.

6. Goldstein, S. — Approximate two-dimensional aerofoil theory Part 1. Velocity distributions for symmetrical aerofoils. C.P. No. 68, 1952.

7. Pankhurst, R.C., Squire, H.B. — Calculated pressure distributions for the RAE 100 - 104 Aerofoil sections. C.P. No. 80, 1952.

8. Burrows, F.M. — Characteristics of the flow field over the mid-upper fuselage of Lancaster PA.474. C. of A. Note No. 36, 1956.

9. Weber, J. — Low speed measurements of pressure distribution near tips of swept back wings at no lift. R.A.E. Report Aero.2318, March 1949.

10. Kuchemann, D. — A simple method for calculating the span and chordwise loading on straight and swept wings of any given aspect ratio at subsonic speeds. R. & M. 2935 1956.

References (Continued)

11. Kuchemann, D., Kettle, D.J. — The effect of endplates on swept wings. C.P. No. 104, 1952.

12. Owen, P.R., Randall, D.G. — Boundary layer transition on a swept back wing: Effect of incidence. R.A.E. TM No. Aero.375, Oct. 1953.

13. Owen, P.R., Randall, D.G. — Boundary layer transition on a swept back wing. R.A.E. TM No. Aero 277, May 1952.

TABLE 1

Measured Static Pressure Distribution

C_p at Station A, $\eta = 0.1255$

$\frac{x}{c}$	$\alpha = 0^\circ$	$\alpha = 2^\circ$		$\alpha = 4^\circ$		$\alpha = 6^\circ$		$\alpha = 8^\circ$		$\alpha = 10^\circ$	
	C_{p_u}	C_{p_u}	C_{p_L}	C_{p_u}	C_{p_L}	C_{p_u}	C_{p_L}	C_{p_u}	C_{p_L}	C_{p_u}	C_{p_L}
0	+0.522	+0.147	+0.528	-0.322	+0.428	-0.834	+0.198	-1.555	-0.167	-2.516	-0.557
0.005	+0.017	-0.573	+0.191	-1.075	+0.404	-1.493	+0.503	-2.328	+0.546	-3.191	+0.530
0.010	-0.030	-0.515	+0.134	-0.926	+0.328	-1.252	+0.437	-1.870	+0.510	-2.497	+0.530
0.015	-0.064	-0.457	+0.076	-0.776	+0.253	-1.011	+0.372	-1.412	+0.472	-1.802	+0.529
0.020	-0.082	-0.441	+0.044	-0.726	+0.216	-0.931	+0.335	-1.273	+0.444	-1.629	+0.514
0.040	-0.110	-0.382	-0.020	-0.598	+0.127	-0.735	+0.235	-0.963	+0.344	-1.224	+0.416
0.100	-0.153	-0.326	-0.065	-0.439	+0.022	-0.565	+0.101	-0.690	+0.193	-0.789	+0.272
0.150	-0.164	-0.306	-0.087	-0.389	-0.023	-0.486	+0.041	-0.591	+0.125	-0.645	+0.191
0.200	-0.231	-0.352	-0.160	-0.423	-0.097	-0.503	-0.034	-0.599	+0.043	-0.638	+0.108
0.319	-0.220	-0.311	-0.166	-0.363	-0.123	-0.413	-0.074	-0.484	-0.016	-0.506	+0.037
0.410	-0.219	-0.285	-0.166	-0.325	-0.131	-0.374	-0.084	-0.422	-0.034	-0.438	+0.007
0.505	-0.182	-0.230	-0.143	-0.261	-0.110	-0.302	-0.081	-0.337	-0.038	-0.348	-0.007
0.594	-0.140	-0.174	-0.105	-0.193	-0.079	-0.230	-0.056	-0.255	-0.013	-0.268	+0.017
0.685	-0.088	-0.114	-0.066	-0.137	-0.041	-0.161	-0.020	-0.179	+0.017	-0.192	+0.040
0.804	-0.030	-0.047	-0.012	-0.055	+0.002	-0.078	+0.016	-0.093	+0.043	-0.099	+0.062
0.900	+0.002	-0.014	+0.010	-0.020	+0.017	-0.030	+0.024	-0.036	+0.041	-0.038	+0.054

TABLE 1 - continued

C_p at Station B, $\eta \doteq 0.251$

$\frac{x}{c}$	$\alpha = 0^\circ$	$\alpha = 2^\circ$		$\alpha = 4^\circ$		$\alpha = 6^\circ$		$\alpha = 8^\circ$		$\alpha = 10^\circ$	
	C_{p_u}	C_{p_u}	C_{p_L}	C_{p_u}	C_{p_L}	C_{p_u}	C_{p_L}	C_{p_u}	C_{p_L}	C_{p_u}	C_{p_L}
0	+0.540	+0.087	+0.532	-0.506	+0.354	-1.179	+0.005	-2.358	-0.602	-3.393	-1.218
0.005	+0.136	-0.497	+0.305	-1.079	+0.490	-1.603	+0.553	-2.492	+0.538	-3.360	+0.458
0.010	+0.015	-0.532	+0.176	-1.010	+0.381	-1.417	+0.490	-2.011	+0.558	-2.559	+0.567
0.015	-0.031	-0.519	+0.115	-0.920	+0.310	-1.219	+0.436	-1.686	+0.533	-2.161	+0.576
0.020	-0.072	-0.507	+0.067	-0.864	+0.256	-1.116	+0.382	-1.546	+0.495	-1.951	+0.550
0.040	-0.128	-0.448	-0.018	-0.685	+0.138	-0.861	+0.257	-1.153	+0.376	-1.438	+0.451
0.100	-0.197	-0.390	-0.094	-0.516	+0.001	-0.667	+0.091	-0.837	+0.195	-0.930	+0.270
0.140	-0.188	-0.350	-0.103	-0.454	-0.023	-0.566	+0.053	-0.702	+0.141	-0.775	+0.216
0.194	-0.245	-0.380	-0.165	-0.458	-0.098	-0.552	-0.032	-0.651	+0.051	-0.695	+0.119
0.3085	-0.210	-0.308	-0.151	-0.367	-0.105	-0.426	-0.055	-0.502	+0.011	-0.531	+0.062
0.4175	-0.220	-0.285	-0.166	-0.328	-0.129	-0.380	-0.091	-0.427	-0.038	-0.446	+0.006
0.512	-0.173	-0.221	-0.130	-0.253	-0.101	-0.295	-0.063	-0.323	-0.023	-0.342	+0.012
0.6065	-0.137	-0.165	-0.101	-0.183	-0.079	-0.199	-0.059	-0.232	-0.017	-0.244	+0.007
0.700	-0.061	-0.086	-0.039	-0.106	-0.018	-0.129	-0.001	-0.145	+0.030	-0.157	+0.053
0.784	-0.017	-0.039	-0.003	-0.055	+0.014	-0.069	+0.027	-0.083	+0.053	-0.090	+0.071
0.910	+0.045	+0.032	+0.052	+0.024	+0.062	+0.015	+0.069	+0.008	+0.085	+0.011	+0.095

TABLE 1 - continued

C_p at Station C, η = 0.3765

$\frac{x}{c}$	$\alpha = 0°$	$\alpha = 2°$		$\alpha = 4°$		$\alpha = 6°$		$\alpha = 8°$		$\alpha = 10°$	
	C_{p_u}	C_{p_u}	C_{p_L}	C_{p_u}	C_{p_L}	C_{p_u}	C_{p_L}	C_{p_u}	C_{p_L}	C_{p_u}	C_{p_L}
0	+0.553	+0.230	+0.471	-0.313	+0.138	-0.964	-0.379	-2.129	-1.188	-3.400	-2.010
0.005	+0.119	-0.580	+0.307	-1.255	+0.496	-1.888	+0.541	-3.049	+0.494	-4.081	+0.372
0.010	-0.017	-0.605	+0.169	-1.149	+0.388	-1.602	+0.494	-2.302	+0.555	-3.004	+0.542
0.015	-0.051	-0.568	+0.113	-1.037	+0.323	-1.374	+0.449	-1.942	+0.540	-2.507	+0.567
0.020	-0.096	-0.569	+0.063	-0.985	+0.269	-1.257	+0.401	-1.780	+0.510	-2.288	+0.561
0.025	-0.117	-0.535	+0.026	-0.887	+0.217	-1.127	+0.346	-1.566	+0.467	-2.008	+0.487
0.075	-0.189	-0.423	-0.063	-0.599	+0.053	-0.788	+0.152	-1.021	+0.267	-1.161	+0.351
0.130	-0.210	-0.389	-0.109	-0.512	-0.022	-0.643	+0.063	-0.803	+0.159	-0.889	+0.236
0.215	-0.204	-0.336	-0.127	-0.420	-0.063	-0.511	+0.003	-0.615	+0.079	-0.668	+0.145
0.312	-0.210	-0.311	-0.150	-0.377	-0.100	-0.439	-0.047	-0.518	+0.017	-0.548	+0.071
0.371	-0.201	-0.282	-0.141	-0.339	-0.100	-0.388	-0.057	-0.455	-0.002	-0.478	+0.042
0.4705	-0.190	-0.251	-0.143	-0.287	-0.107	-0.334	-0.071	-0.365	-0.025	-0.388	+0.009
0.5715	-0.134	-0.167	-0.096	-0.195	-0.071	-0.225	-0.045	-0.251	+0.001	-0.270	+0.030
0.6915	-0.055	-0.083	-0.033	-0.102	-0.013	-0.124	+0.006	-0.140	+0.035	-0.151	+0.057
0.800	-0.014	-0.028	0.000	-0.045	+0.016	-0.057	+0.029	-0.070	+0.053	-0.073	+0.070
0.900	+0.042	+0.028	+0.048	+0.018	+0.056	+0.012	+0.064	+0.004	+0.080	+0.012	+0.091

TABLE 1 - continued

C_p at Station D, η = 0.502

$\frac{x}{c}$	$\alpha = 0°$	$\alpha = 2°$		$\alpha = 4°$		$\alpha = 6°$		$\alpha = 8°$		$\alpha = 10°$	
	C_{p_u}	C_{p_u}	C_{p_L}	C_{p_u}	C_{p_L}	C_{p_u}	C_{p_L}	C_{p_u}	C_{p_L}	C_{p_u}	C_{p_L}
0	+0.562	+0.231	+0.476	-0.352	+0.137	-1.053	-0.394	-2.294	-1.225	-3.600	-2.083
0.005	+0.167	-0.678	+0.305	-1.449	+0.502	-2.185	+0.528	-3.393	+0.444	-4.454	+0.274
0.010	+0.054	-0.656	+0.179	-1.269	+0.408	-3.771	+0.509	-2.466	+0.553	-3.235	+0.512
0.015	-0.070	-0.695	+0.067	-1.218	+0.309	-1.654	+0.443	-2.356	+0.530	-3.009	+0.549
0.020	-0.086	-0.638	+0.044	-1.108	+0.264	-1.435	+0.403	-2.018	+0.510	-2.569	+0.549
0.040	-0.128	-0.511	-0.025	-0.822	+0.157	-1.040	+0.282	-1.404	+0.398	-1.752	+0.467
0.100	-0.187	-0.422	-0.085	-0.576	+0.022	-0.746	+0.116	-0.956	+0.224	-1.078	+0.307
0.158	-0.196	-0.381	-0.115	-0.494	-0.031	-0.605	+0.044	-0.762	+0.138	-0.841	+0.210
0.212	-0.209	-0.353	-0.129	-0.442	-0.061	-0.531	+0.004	-0.650	+0.086	-0.710	+0.153
0.310	-0.220	-0.335	-0.167	-0.401	-0.113	-0.473	-0.060	-0.552	+0.005	-0.587	+0.063
0.369	-0.218	-0.308	-0.163	-0.363	-0.121	-0.411	-0.073	-0.489	-0.013	-0.511	+0.035
0.4775	-0.191	-0.255	-0.149	-0.294	-0.117	-0.336	-0.079	-0.376	-0.030	-0.394	+0.002
0.600	-0.115	-0.155	-0.089	-0.176	-0.063	-0.207	-0.040	-0.233	0.000	-0.248	+0.028
0.700	-0.051	-0.078	-0.031	-0.097	-0.013	-0.116	+0.004	-0.131	+0.036	-0.140	+0.055
0.800	-0.020	-0.040	-0.007	-0.052	+0.004	-0.064	+0.012	-0.072	+0.039	-0.075	+0.051
0.910	+0.033	+0.018	+0.040	+0.014	+0.046	+0.010	+0.051	+0.003	+0.065	+0.011	+0.075

TABLE 1 - continued

C_p at Station E, $\eta = 0.6275$

$\frac{x}{c}$	$\alpha = 0^\circ$	$\alpha = 2^\circ$		$\alpha = 4^\circ$		$\alpha = 6^\circ$		$\alpha = 8^\circ$		$\alpha = 10^\circ$	
	C_{p_u}	C_{p_u}	C_{p_L}	C_{p_u}	C_{p_L}	C_{p_u}	C_{p_L}	C_{p_u}	C_{p_L}	C_{p_u}	C_{p_L}
0	+0.540	+0.058	+0.481	-0.689	+0.149	-1.569	-0.422	-3.136	-1.333	-4.446	-2.302
0.005	+0.115	-0.643	+0.319	-1.413	+0.505	-2.150	+0.518	-3.421	+0.419	-4.275	+0.235
0.010	-0.019	-0.661	+0.186	-1.300	+0.411	-1.829	+0.501	-2.655	+0.517	-3.487	+0.453
0.015	-0.080	-0.673	+0.115	-1.228	+0.344	-1.677	+0.467	-2.386	+0.540	-3.077	+0.535
0.020	-0.136	-0.657	+0.054	-1.153	+0.283	-1.534	+0.417	-2.165	+0.512	-2.759	+0.541
0.040	-0.170	-0.560	-0.040	-0.891	+0.151	-1.138	+0.283	-1.530	+0.404	-1.911	+0.471
0.100	-0.190	-0.409	-0.067	-0.572	+0.041	-0.753	+0.134	-0.977	+0.243	-1.118	+0.323
0.150	-0.210	-0.388	-0.110	-0.513	-0.022	-0.640	+0.063	-0.807	+0.157	-0.901	+0.231
0.210	-0.218	-0.360	-0.136	-0.455	-0.064	-0.543	+0.003	-0.675	+0.086	-0.738	+0.154
0.3035	-0.247	-0.351	-0.177	-0.417	-0.121	-0.490	-0.067	-0.574	+0.002	-0.610	+0.060
0.368	-0.201	-0.282	-0.143	-0.328	-0.101	-0.373	-0.060	-0.449	-0.003	-0.486	+0.043
0.486	-0.150	-0.213	-0.109	-0.238	-0.081	-0.255	-0.053	-0.324	-0.008	-0.361	+0.025
0.600	-0.109	-0.143	-0.077	-0.164	-0.054	-0.194	-0.036	-0.219	0.000	-0.235	+0.025
0.681	-0.055	-0.077	-0.030	-0.097	-0.015	-0.119	+0.003	-0.136	+0.030	-0.145	+0.051
0.800	-0.008	-0.024	+0.003	-0.037	+0.013	-0.048	+0.021	-0.060	+0.040	-0.062	+0.055
0.900	+0.045	+0.029	+0.051	+0.024	+0.057	+0.014	+0.067	+0.006	+0.076	+0.010	+0.088

TABLE 1 - continued

C_p at Station F, η = 0.753

$\frac{x}{c}$	α = 0°	α = 2°		α = 4°		α = 6°		α = 8°		α = 10°	
	C_{p_u}	C_{p_u}	C_{p_L}	C_{p_u}	C_{p_L}	C_{p_u}	C_{p_L}	C_{p_u}	C_{p_L}	C_{p_u}	C_{p_L}
0	+0.549	+0.145	+0.461	-0.553	+0.094	-1.404	-0.505	-2.910	-1.465	-4.412	-2.408
0.005	+0.038	-0.773	+0.273	-1.590	+0.493	-2.358	+0.531	-3.579	+0.457	-4.498	+0.287
0.010	-0.049	-0.703	+0.160	-1.361	+0.393	-1.904	+0.491	-2.694	+0.518	-3.494	+0.466
0.015	-0.080	-0.631	+0.111	-1.157	+0.336	-1.554	+0.453	-2.275	+0.524	-2.896	+0.524
0.020	-0.156	-0.640	+0.036	-1.163	+0.274	-1.555	+0.406	-2.147	+0.502	-2.696	+0.530
0.040	-0.165	-0.537	-0.022	-0.865	+0.165	-1.112	+0.297	-1.502	+0.417	-1.885	+0.490
0.100	-0.209	-0.435	-0.086	-0.598	+0.024	-0.782	+0.121	-1.012	+0.228	-1.150	+0.314
0.150	-0.222	-0.399	-0.120	-0.527	-0.031	-0.647	+0.050	-0.818	+0.143	-0.912	+0.219
0.200	-0.231	-0.375	-0.139	-0.473	-0.070	-0.567	-0.003	-0.695	+0.080	-0.761	+0.150
0.3065	-0.219	-0.318	-0.154	-0.382	-0.109	-0.443	-0.059	-0.525	+0.005	-0.563	+0.059
0.3675	-0.208	-0.285	-0.149	-0.335	-0.111	-0.387	-0.070	-0.455	-0.017	-0.461	+0.028
0.500	-0.146	-0.194	-0.109	-0.220	-0.086	-0.264	-0.060	-0.296	-0.020	-0.315	+0.005
0.600	-0.099	-0.127	-0.073	-0.144	-0.057	-0.171	-0.041	-0.186	-0.007	-0.208	+0.013
0.6945	-0.038	-0.060	-0.023	-0.075	-0.011	-0.090	+0.001	-0.111	+0.024	-0.122	+0.039
0.800	-0.007	-0.021	+0.001	-0.031	+0.007	-0.048	+0.014	-0.064	+0.029	-0.072	+0.036
0.900	+0.049	+0.036	+0.054	+0.027	+0.055	+0.015	+0.063	+0.002	+0.071	-0.002	+0.076

TABLE 1 - continued

C_p at Station G, η = 0.8785

$\frac{x}{c}$	$\alpha = 0^\circ$	$\alpha = 2^\circ$		$\alpha = 4^\circ$		$\alpha = 6^\circ$		$\alpha = 8^\circ$		$\alpha = 10^\circ$	
	C_{p_u}	C_{p_u}	C_{p_L}	C_{p_u}	C_{p_L}	C_{p_u}	C_{p_L}	C_{p_u}	C_{p_L}	C_{p_u}	C_{p_L}
0	+0.538	+0.238	+0.417	-0.352	+0.002	-1.089	-0.604	-2.404	-1.543	-3.665	-2.491
0.005	+0.011	-0.736	+0.233	-1.481	+0.451	-2.234	+0.507	-3.486	+0.469	-4.373	+0.336
0.010	-0.114	-0.741	+0.101	-1.325	+0.347	-1.836	+0.462	-2.697	+0.513	-3.421	+0.484
0.015	-0.129	-0.663	+0.061	-1.182	+0.288	-1.568	+0.411	-2.232	+0.488	-2.828	+0.501
0.020	-0.178	-0.650	+0.002	-1.120	+0.226	-1.483	+0.359	-2.064	+0.460	-2.564	+0.496
0.040	-0.202	-0.543	-0.019	-0.823	+0.129	-1.096	+0.252	-1.486	+0.366	-1.739	+0.436
0.087	-0.192	-0.410	-0.076	-0.573	+0.029	-0.744	+0.119	-0.970	+0.216	-1.111	+0.290
0.150	-0.214	-0.365	-0.124	-0.473	-0.049	-0.585	+0.015	-0.730	+0.098	-0.812	+0.157
0.200	-0.196	-0.316	-0.124	-0.399	-0.068	-0.485	-0.014	-0.598	+0.049	-0.662	+0.101
0.300	-0.191	-0.274	-0.141	-0.328	-0.102	-0.392	-0.066	-0.469	-0.018	-0.508	+0.021
0.400	-0.236	-0.284	-0.187	-0.310	-0.163	-0.365	-0.137	-0.406	-0.092	-0.446	-0.061
0.505	-0.136	-0.169	-0.096	-0.192	-0.090	-0.230	-0.075	-0.265	-0.043	-0.297	-0.026
0.581	-0.081	-0.107	-0.063	-0.129	-0.050	-0.160	-0.041	-0.192	-0.016	-0.223	-0.009
0.662	-0.046	-0.065	-0.039	-0.081	-0.031	-0.112	-0.028	-0.141	-0.014	-0.167	-0.003
0.7905	-0.007	-0.022	-0.006	-0.033	-0.005	-0.063	-0.011	-0.091	-0.001	-0.112	+0.011
0.900	+0.043	+0.024	+0.043	+0.013	+0.040	-0.013	+0.038	-0.041	+0.040	-0.052	+0.039

TABLE 1 - continued

C_p at Station H, η = 0.9605

$\frac{x}{c}$	$\alpha = 0°$	$\alpha = 2°$		$\alpha = 4°$		$\alpha = 6°$		$\alpha = 8°$		$\alpha = 10°$	
	C_{p_u}	C_{p_u}	C_{p_L}	C_{p_u}	C_{p_L}	C_{p_u}	C_{p_L}	C_{p_u}	C_{p_L}	C_{p_u}	C_{p_L}
0	+0.156	-0.305	+0.109	-0.780	-0.123	-1.513	-0.514	-2.735	-1.178	-4.026	-1.861
0.005	-0.009	-0.427	+0.056	-0.926	-0.035	-1.536	-0.269	-2.548	-0.659	-3.587	-1.172
0.010	-0.093	-0.550	+0.003	-1.072	+0.053	-1.559	-0.023	-2.361	-0.219	-3.148	-0.483
0.015	-0.157	-0.500	-0.041	-0.887	+0.020	-1.330	-0.033	-1.903	-0.189	-2.679	-0.368
0.020	-0.104	-0.462	-0.010	-0.858	+0.072	-1.204	+0.072	-1.772	+0.008	-2.406	-0.109
0.040	-0.125	-0.392	-0.027	-0.629	+0.041	-0.893	+0.096	-1.327	+0.089	-1.470	+0.055
0.100	-0.185	-0.369	-0.106	-0.509	-0.050	-0.649	-0.016	-0.902	+0.013	-1.068	+0.021
0.150	-0.173	-0.314	-0.107	-0.416	-0.067	-0.512	-0.041	-0.720	-0.015	-0.857	-0.005
0.200	-0.186	-0.302	-0.130	-0.386	-0.100	-0.463	-0.078	-0.638	-0.054	-0.757	-0.041
0.300	-0.229	-0.310	-0.183	-0.370	-0.176	-0.434	-0.165	-0.564	-0.153	-0.666	-0.153
0.400	-0.168	-0.217	-0.147	-0.264	-0.140	-0.341	-0.148	-0.422	-0.142	-0.517	-0.153
0.500	-0.115	-0.165	-0.096	-0.209	-0.098	-0.291	-0.109	-0.388	-0.109	-0.469	-0.122
0.600	-0.072	-0.113	-0.060	-0.161	-0.060	-0.251	-0.076	-0.337	-0.075	-0.411	-0.088
0.700	-0.029	-0.074	-0.025	-0.129	-0.027	-0.211	-0.033	-0.306	-0.036	-0.408	-0.042
0.800	-0.010	-0.052	-0.011	-0.099	-0.014	-0.177	-0.009	-0.295	-0.003	-0.467	-0.031
0.900	+0.029	-0.010	+0.026	-0.050	+0.017	-0.132	+0.005	-0.274	+0.006	-0.432	-0.001

TABLE 2

Measured Loading Distribution

ΔC_p at Station A, η = 0.1255

$\frac{x}{c}$	$\alpha = 2^{\circ}$	$\alpha = 4^{\circ}$	$\alpha = 6^{\circ}$	$\alpha = 8^{\circ}$	$\alpha = 10^{\circ}$
0	-0.381	-0.750	-1.032	-1.368	-1.959
0.005	-0.764	-1.479	-1.996	-2.876	-3.721
0.010	-0.649	-1.254	-1.689	-2.380	-3.027
0.015	-0.533	-1.029	-1.383	-1.884	-2.331
0.020	-0.485	-0.942	-1.266	-1.717	-2.143
0.040	-0.362	-0.725	-0.970	-1.307	-1.642
0.100	-0.261	-0.461	-0.666	-0.883	-1.061
0.150	-0.219	-0.366	-0.527	-0.716	-0.836
0.200	-0.192	-0.326	-0.469	-0.642	-0.746
0.319	-0.145	-0.240	-0.339	-0.468	-0.543
0.410	-0.119	-0.194	-0.294	-0.388	-0.445
0.505	-0.087	-0.151	-0.221	-0.299	-0.341
0.594	-0.069	-0.119	-0.174	-0.242	-0.285
0.685	-0.048	-0.096	-0.141	-0.196	-0.232
0.804	-0.035	-0.057	-0.094	-0.136	-0.161
0.900	-0.024	-0.037	-0.054	-0.077	-0.092

TABLE 2 - continued

ΔC_p at Station B, η = 0.251

$\frac{x}{c}$	$\alpha = 2^\circ$	$\alpha = 4^\circ$	$\alpha = 6^\circ$	$\alpha = 8^\circ$	$\alpha = 10^\circ$
0	-0.445	-0.860	-1.184	-1.756	-2.175
0.005	-0.802	-1.569	-2.156	-3.030	-3.818
0.010	-0.708	-1.391	-1.907	-2.669	-3.126
0.015	-0.634	-1.230	-1.655	-1.219	-2.737
0.020	-0.574	-1.120	-1.498	-2.041	-2.501
0.040	-0.430	-0.823	-1.118	-1.529	-1.889
0.100	-0.296	-0.517	-0.758	-1.032	-1.200
0.140	-0.247	-0.431	-0.619	-0.843	-0.991
0.194	-0.215	-0.360	-0.520	-0.702	-0.814
0.3085	-0.157	-0.262	-0.371	-0.513	-0.593
0.4175	-0.119	-0.199	-0.289	-0.389	-0.452
0.512	-0.091	-0.152	-0.232	-0.300	-0.354
0.6065	-0.064	-0.104	-0.140	-0.215	-0.251
0.700	-0.047	-0.088	-0.128	-0.175	-0.210
0.784	-0.036	-0.069	-0.096	-0.136	-0.161
0.910	-0.020	-0.038	-0.054	-0.077	-0.084

TABLE 2 - continued

ΔC_p at Station C, η = 0.3765

$\frac{x}{c}$	$\alpha = 2^\circ$	$\alpha = 4^\circ$	$\alpha = 6^\circ$	$\alpha = 8^\circ$	$\alpha = 10^\circ$
0	-0.241	-0.451	-0.585	-0.941	-1.390
0.005	-0.887	-1.751	-2.429	-3.543	-4.453
0.010	-0.774	-1.537	-2.096	-2.857	-3.546
0.015	-0.681	-1.360	-1.823	-2.482	-3.074
0.020	-0.632	-1.254	-1.658	-2.290	-2.849
0.025	-0.561	-1.104	-1.473	-2.033	-2.495
0.075	-0.360	-0.652	-0.940	-1.288	-1.512
0.130	-0.280	-0.490	-0.706	-0.962	-1.125
0.215	-0.209	-0.357	-0.514	-0.694	-0.813
0.312	-0.161	-0.277	-0.392	-0.535	-0.619
0.371	-0.141	-0.239	-0.331	-0.453	-0.520
0.4705	-0.108	-0.180	-0.263	-0.340	-0.397
0.5715	-0.071	-0.124	-0.180	-0.252	-0.300
0.6915	-0.050	-0.089	-0.130	-0.175	-0.208
0.800	-0.028	-0.061	-0.086	-0.123	-0.143
0.900	-0.020	-0.038	-0.052	-0.076	-0.079

TABLE 2 - continued

ΔC_p at Station D, η = 0.502

$\frac{x}{c}$	$\alpha = 2^{\circ}$	$\alpha = 4^{\circ}$	$\alpha = 6^{\circ}$	$\alpha = 8^{\circ}$	$\alpha = 10^{\circ}$
0	-0.245	-0.489	-0.659	-1.069	-1.517
0.005	-0.983	-1.951	-2.713	-3.837	-4.728
0.010	-0.835	-1.677	-4.280	-3.019	-3.747
0.015	-0.762	-1.527	-2.097	-2.886	-3.558
0.020	-0.682	-1.372	-1.838	-2.528	-3.118
0.040	-0.486	-0.979	-1.322	-1.802	-2.219
0.100	-0.337	-0.598	-0.862	-1.180	-1.385
0.158	-0.266	-0.463	-0.649	-0.900	-1.051
0.212	-0.224	-0.381	-0.535	-0.736	-0.863
0.310	-0.168	-0.288	-0.413	-0.557	-0.650
0.369	-0.145	-0.242	-0.338	-0.476	-0.546
0.4775	-0.106	-0.177	-0.257	-0.346	-0.396
0.600	-0.066	-0.113	-0.167	-0.233	-0.276
0.700	-0.047	-0.084	-0.120	-0.167	-0.195
0.800	-0.033	-0.056	-0.076	-0.111	-0.126
0.910	-0.022	-0.032	-0.041	-0.062	-0.064

TABLE 2 - continued

ΔC_p at Station E, η = 0.6275

$\frac{x}{c}$	$\alpha = 2^\circ$	$\alpha = 4^\circ$	$\alpha = 6^\circ$	$\alpha = 8^\circ$	$\alpha = 10^\circ$
0	-0.423	-0.838	-1.147	-1.803	-2.144
0.005	-0.962	-1.918	-2.668	-3.840	-4.510
0.010	-0.847	-1.711	-2.330	-3.172	-3.940
0.015	-0.788	-1.572	-2.144	-2.926	-3.612
0.020	-0.711	-1.436	-1.951	-2.677	-3.300
0.040	-0.520	-1.042	-1.421	-1.934	-2.382
0.100	-0.342	-0.613	-0.887	-1.220	-1.441
0.150	-0.278	-0.491	-0.703	-0.964	-1.132
0.210	-0.224	-0.391	-0.546	-0.761	-0.892
0.3035	-0.174	-0.296	-0.423	-0.576	-0.670
0.368	-0.139	-0.227	-0.313	-0.446	-0.529
0.486	-0.104	-0.157	-0.202	-0.316	-0.386
0.600	-0.066	-0.110	-0.158	-0.219	-0.260
0.681	-0.047	-0.082	-0.122	-0.166	-0.196
0.800	-0.027	-0.050	-0.069	-0.100	-0.117
0.900	-0.022	-0.033	-0.053	-0.070	-0.078

TABLE 2 - continued

ΔC_p at Station F, $\eta = 0.753$

$\frac{x}{c}$	$\alpha = 2^\circ$	$\alpha = 4^\circ$	$\alpha = 6^\circ$	$\alpha = 8^\circ$	$\alpha = 10^\circ$
0	-0.316	-0.647	-0.899	-1.445	-2.004
0.005	-1.046	-2.083	-2.889	-4.036	-4.785
0.010	-0.863	-1.754	-2.395	-3.212	-3.960
0.015	-0.742	-1.493	-2.007	-2.799	-3.420
0.020	-0.676	-1.437	-1.961	-2.649	-3.226
0.040	-0.515	-1.030	-1.409	-1.919	-2.375
0.100	-0.349	-0.622	-0.903	-1.240	-1.464
0.150	-0.279	-0.496	-0.697	-0.961	-1.131
0.200	-0.236	-0.403	-0.564	-0.775	-0.911
0.3065	-0.164	-0.273	-0.384	-0.530	-0.622
0.3675	-0.136	-0.224	-0.317	-0.438	-0.509
0.500	-0.085	-0.134	-0.204	-0.276	-0.320
0.600	-0.054	-0.087	-0.130	-0.179	-0.221
0.6945	-0.037	-0.064	-0.091	-0.135	-0.161
0.800	-0.022	-0.038	-0.062	-0.093	-0.108
0.900	-0.018	-0.028	-0.048	-0.069	-0.078

TABLE 2 - continued

ΔC_p at Station G, $\eta = 0.8785$

$\frac{x}{c}$	$\alpha = 2^\circ$	$\alpha = 4^\circ$	$\alpha = 6^\circ$	$\alpha = 8^\circ$	$\alpha = 10^\circ$
0	-0.179	-0.354	-0.485	-0.861	-1.174
0.005	-0.969	-1.932	-2.741	-3.955	-4.709
0.010	-0.842	-1.672	-2.298	-3.210	-3.905
0.015	-0.724	-1.470	-1.979	-2.720	-3.329
0.020	-0.652	-1.346	-1.842	-2.524	-3.060
0.040	-0.524	-0.952	-1.348	-1.852	-2.175
0.087	-0.334	-0.602	-0.863	-1.186	-1.401
0.150	-0.241	-0.424	-0.600	-0.828	-0.969
0.200	-0.192	-0.331	-0.471	-0.647	-0.763
0.300	-0.133	-0.226	-0.326	-0.451	-0.529
0.400	-0.097	-0.147	-0.228	-0.314	-0.385
0.505	-0.073	-0.102	-0.155	-0.222	-0.271
0.581	-0.044	-0.079	-0.119	-0.174	-0.214
0.682	-0.026	-0.050	-0.084	-0.127	-0.164
0.7905	-0.016	-0.028	-0.052	-0.090	-0.123
0.900	-0.019	-0.027	-0.051	-0.081	-0.091

TABLE 4

Measured Local Lift Coefficients and Aerodynamic Centre Positions.

C_L

α°	η							
	0.1255	0.251	0.3765	0.502	0.6275	0.753	0.8785	0.9605
2	0.125	0.135	0.142	0.149	0.150	0.145	0.126	0.111
4	0.221	0.240	0.256	0.268	0.270	0.261	0.223	0.198
6	0.314	0.340	0.361	0.386	0.377	0.370	0.323	0.297
8	0.429	0.462	0.496	0.519	0.528	0.512	0.455	0.453
10	0.513	0.552	0.587	0.613	0.631	0.611	0.544	0.572

h/c

α°	η							
	0.1255	0.251	0.3765	0.502	0.6725	0.753	0.8785	0.9605
2	0.269	0.257	0.249	0.247	0.239	0.227	0.214	0.271
4	0.261	0 .251	0.244	0.235	0.225	0.213	0.201	0.275
6	0.269	0.254	0.247	0.231	0.227	0.219	0.212	0.304
8	0.271	0.258	0.247	0.239	0.229	0.222	0.219	0.323
10	0.266	0.252	0.243	0.234	0.227	0.219	0.222	0.344

T A B L E 5

Coefficients of Total Lift from Pressure Measurements

α°	$\bar{C}_L$
2	0.134
4	0.244
6	0.343
8	0.474
10	0.565

T A B L E 6

Chordwise Loading (Mid semi-span)

(a) [illegible].perimental

$\frac{x}{c}$	$-\frac{\Delta C_p}{C_L}$		
	$\alpha = 2^\circ$	$\alpha = 4^\circ$	$\alpha - 6^\circ$
0	1.64	1.83	1.71
0.005	6.60	7.28	7.03
0.010	5.61	6.26	11.09
0.015	5.12	5.70	5.44
0.020	4.58	5.12	4.76
0.040	3.27	3.65	3.43
0.100	2.26	2.23	2.24
0.158	1.79	1.73	1.58
0.212	1.50	1.42	1.39
0.310	1.13	1.07	1.07
0.369	0.97	0.90	0.88
0.4775	0.71	0.66	0.67
0.600	0.44	0.42	0.43
0.700	0.32	0.31	0.31
0.800	0.22	0.21	0.20
0.910	0.15	0.12	0.11

(b) Theoretical

$\frac{x}{c}$	$-\frac{\Delta C_p}{C_L}$
0	∞
0.005	9.78
0.010	6.77
0.015	5.46
0.020	4.68
0.050	2.84
0.100	1.92
0.200	1.25
0.300	0.94
0.400	0.75
0.500	0.60
0.600	0.49
0.700	0.39
0.800	0.29
0.900	0.19
1.000	0

TABLE 7

Spanwise Loading

(a) Experimental

η	$\frac{dC_L}{d\alpha}$	$C_L c / \overline{C_L c}$		
		$\alpha = 2^\circ$	$\alpha = 4^\circ$	$\alpha = 6^\circ$
0.1255	2.84	1.14	1.11	1.12
0.251	3.07	1.16	1.13	1.14
0.3765	3.27	1.14	1.12	1.13
0.502	3.44	1.11	1.10	1.12
0.6275	3.47	1.04	1.02	1.02
0.753	3.32	0.92	0.91	0.92
0.8785	2.90	0.73	0.71	0.73
0.9605	2.61	0.56	0.55	0.58

(b) Theoretical

η	C_L/α		$C_L c / \overline{C_L c}$	
	Linear Theory	With tip-vortex effect	Linear Theory	With tip-vortex effect
0	2.73	2.74	1.20	1.18
0.1951	3.00	3.01	1.20	1.18
0.3827	3.18	3.19	1.15	1.13
0.5556	3.24	3.27	1.05	1.04
0.7071	3.18	3.25	0.94	0.94
0.8315	2.90	3.01	0.78	0.80
0.9239	2.33	2.57	0.59	0.63
0.9808	1.61	2.22	0.32	0.44
1.0000	0	2.18	0	0.30

TABLE 8

Location of the Transition Fronts

SPANWISE STATION	η	END OF TRANSITION REGION AS A PERCENTAGE OF THE LOCAL CHORD									
		$R_e = 0.88 \times 10^6$ / ft.					$R_e = 1.37 \times 10^6$ / ft.				
		$\alpha = 0^o$	$\alpha = 2^o$		$\alpha = 4^o$		$\alpha = 0^o$	$\alpha = 2^o$		$\alpha = 4^o$	
		U.S.	U.S.	L.S.	U.S.	L.S.	U.S.	U.S.	L.S.	U.S.	L.S.
A	0.1255	38	23	21	11	5	18	20	5	<5	<5
B	0.251	19	12	16	10	<5	7	8	<5	5	<5
C	0.3765	20	23	20	15	13	13	16	10	11	<5
D	0.502	45	29	42	20	20	19	22	16	16	<5
E	0.6275	50	30	33	17	19	26	20	16	10	<5
F	0.753	46	28	41	10	12	26	18	5	5	<5
G	0.8785	33	29	29	12	20	21	20	<5	12	<5
H	0.9605	-	-	-	-	-	-	-	-	-	-

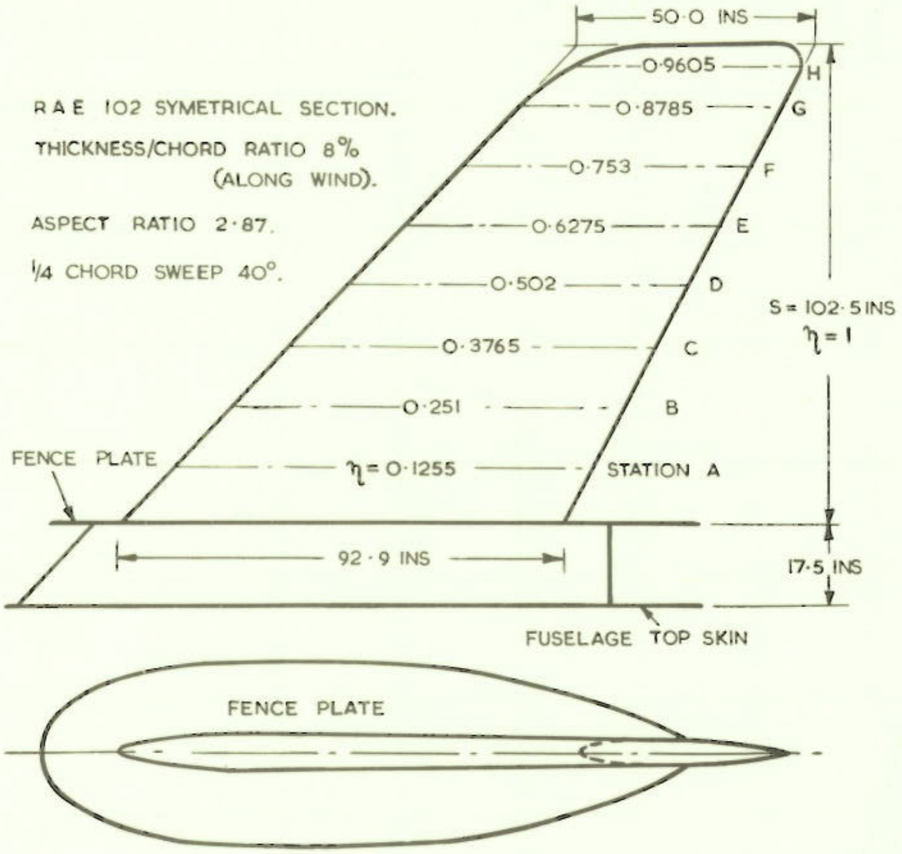

FIG. 1. GEOMETRY OF WING AND BOUNDARY LAYER FENCE.

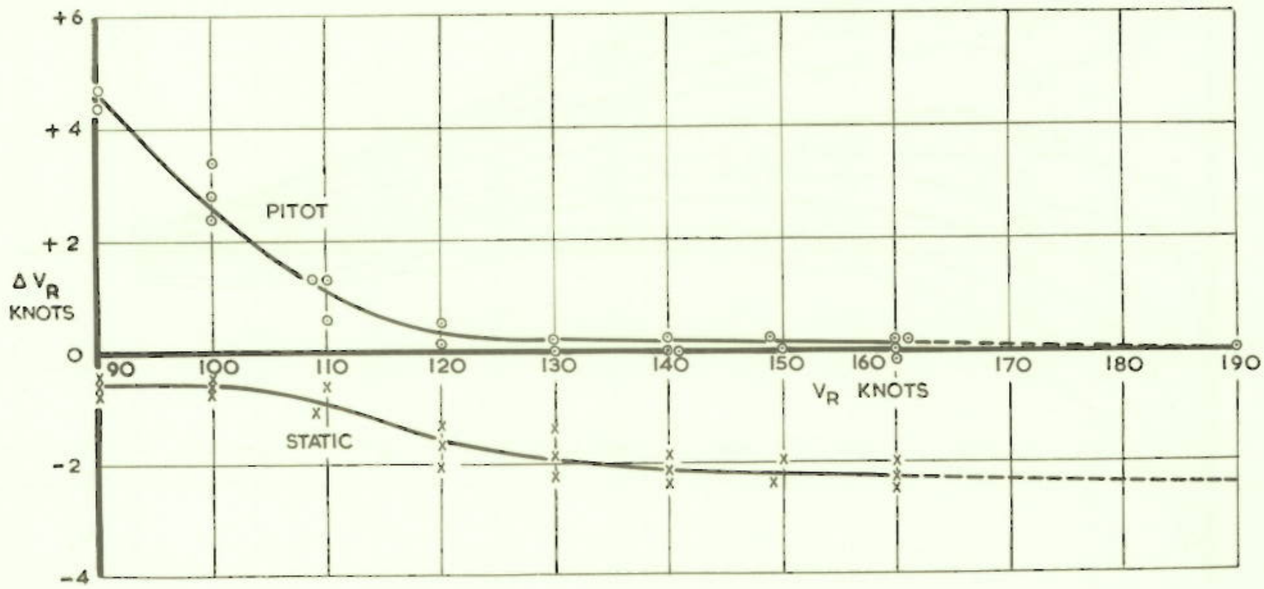

FIG. 2. PRESSURE ERROR CORRECTION CURVES FOR LANCASTER PA 474.

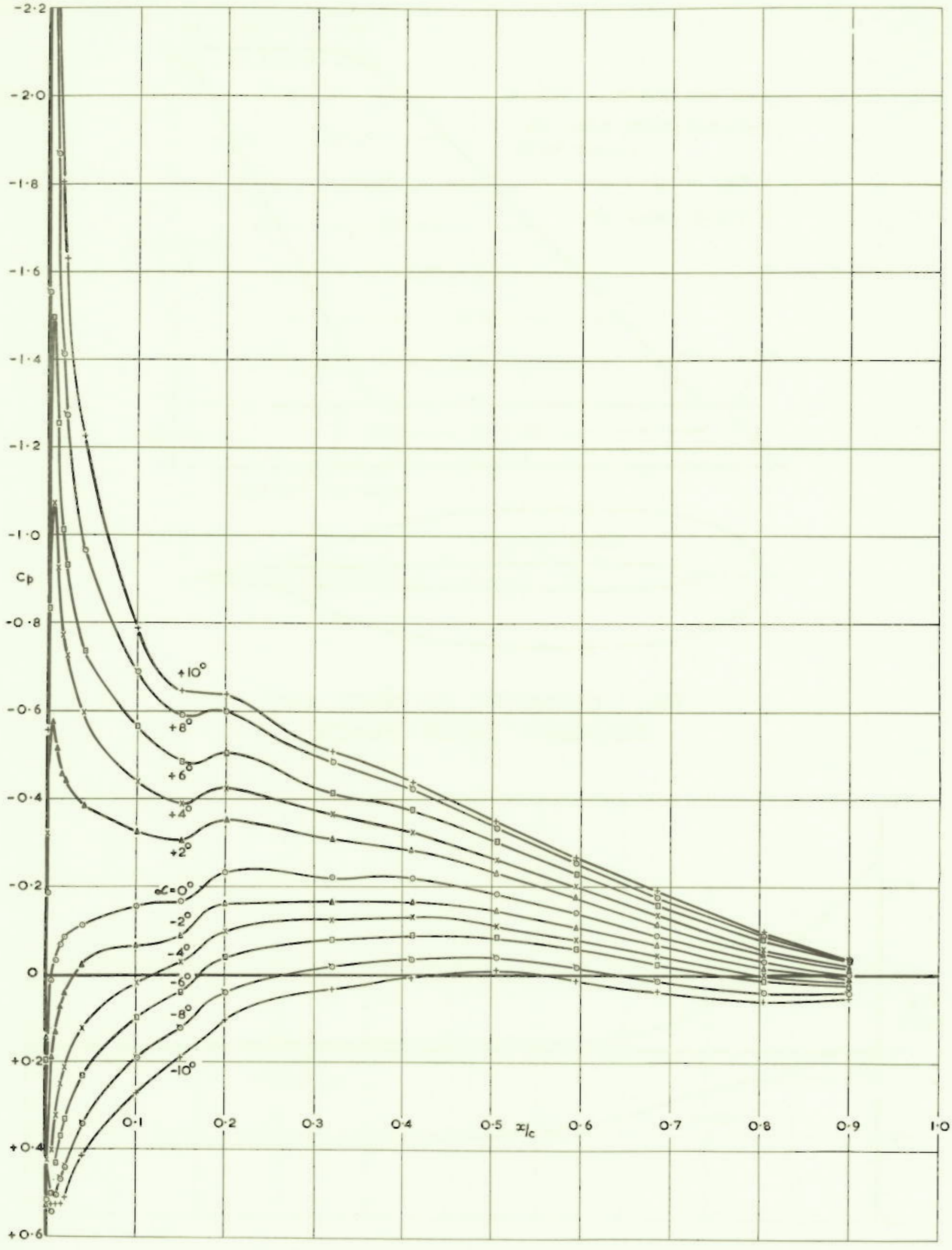

FIG. 3a. STATIC PRESSURE DISTRIBUTION FOR $R_e = 0 \cdot 88 \times 10^6 - 1 \cdot 86 \times 10^6$ PER FT.

STATION A $- \eta = 0 \cdot 1255$.

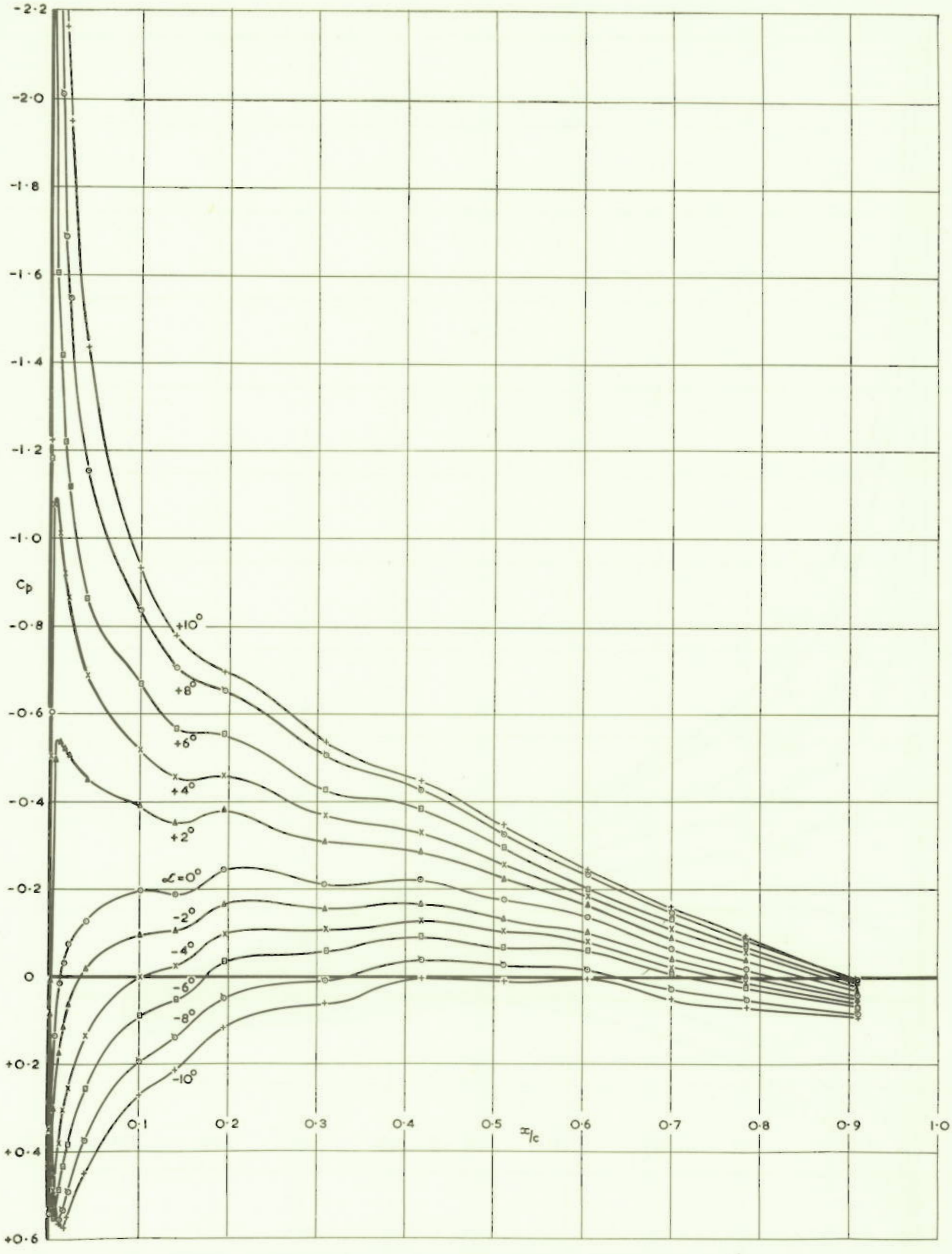

FIG. 3b. STATIC PRESSURE DISTRIBUTION FOR $R_e = 0{\cdot}88 \times 10^6 - 1{\cdot}86 \times 10^6$ PER FT.
STATION B $- \eta = 0{\cdot}251$

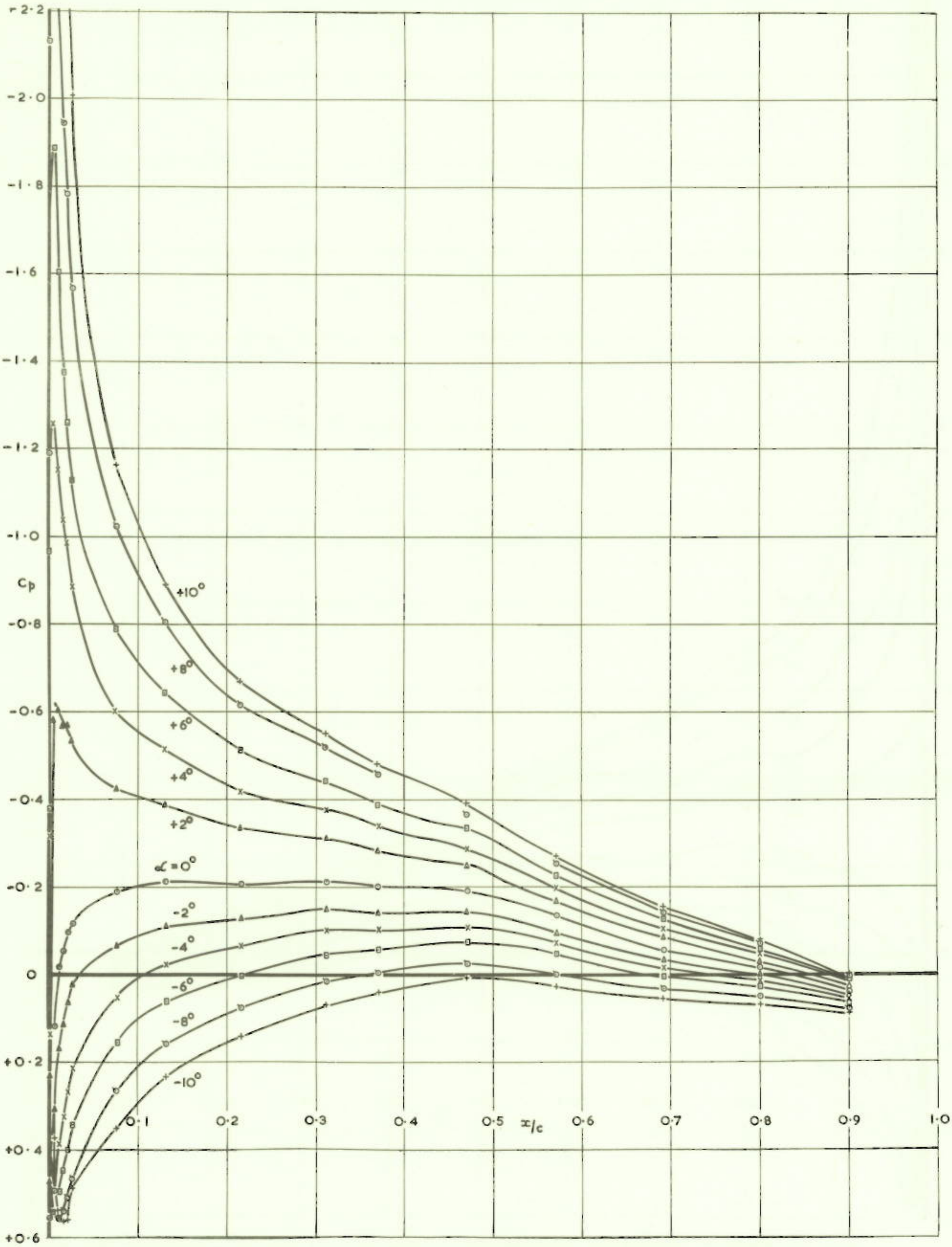

FIG. 3c. STATIC PRESSURE DISTRIBUTION FOR R_e=0·88 x 10^6 - 1·86 x 10^6 PER FT.
STATION C - η = 0·3765

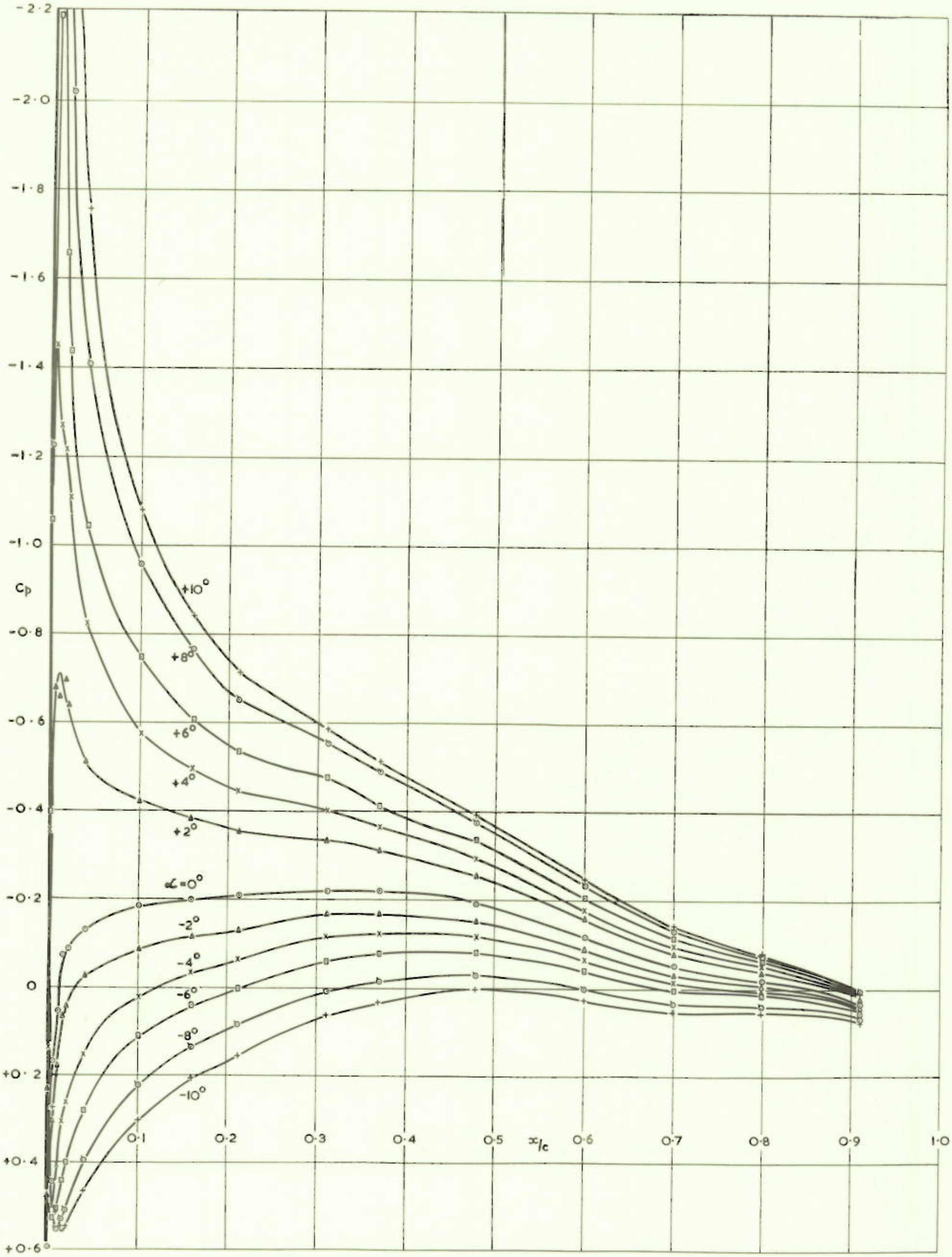

FIG. 3d. STATIC PRESSURE DISTRIBUTION FOR $R_{\bar{c}} = 0 \cdot 88 \times 10^6 - 1 \cdot 86 \times 10^6$ PER FT.
STATION D – $\eta = 0 \cdot 502$

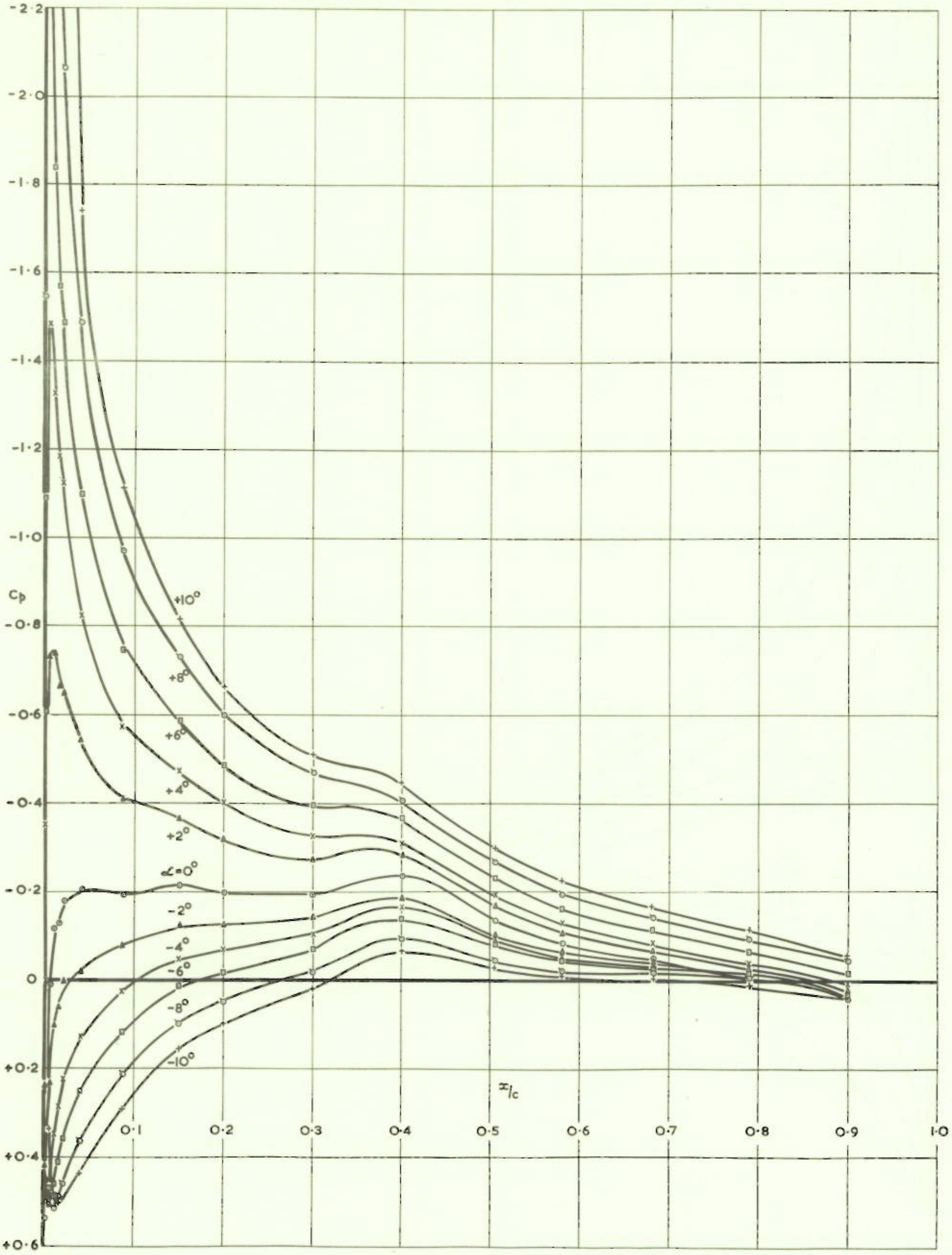

FIG. 3g. STATIC PRESSURE DISTRIBUTION FOR $R_e = 0 \cdot 88 \times 10^6 - 1 \cdot 86 \times 10^6$ PER FT.
STATION G - η = 0·8785.

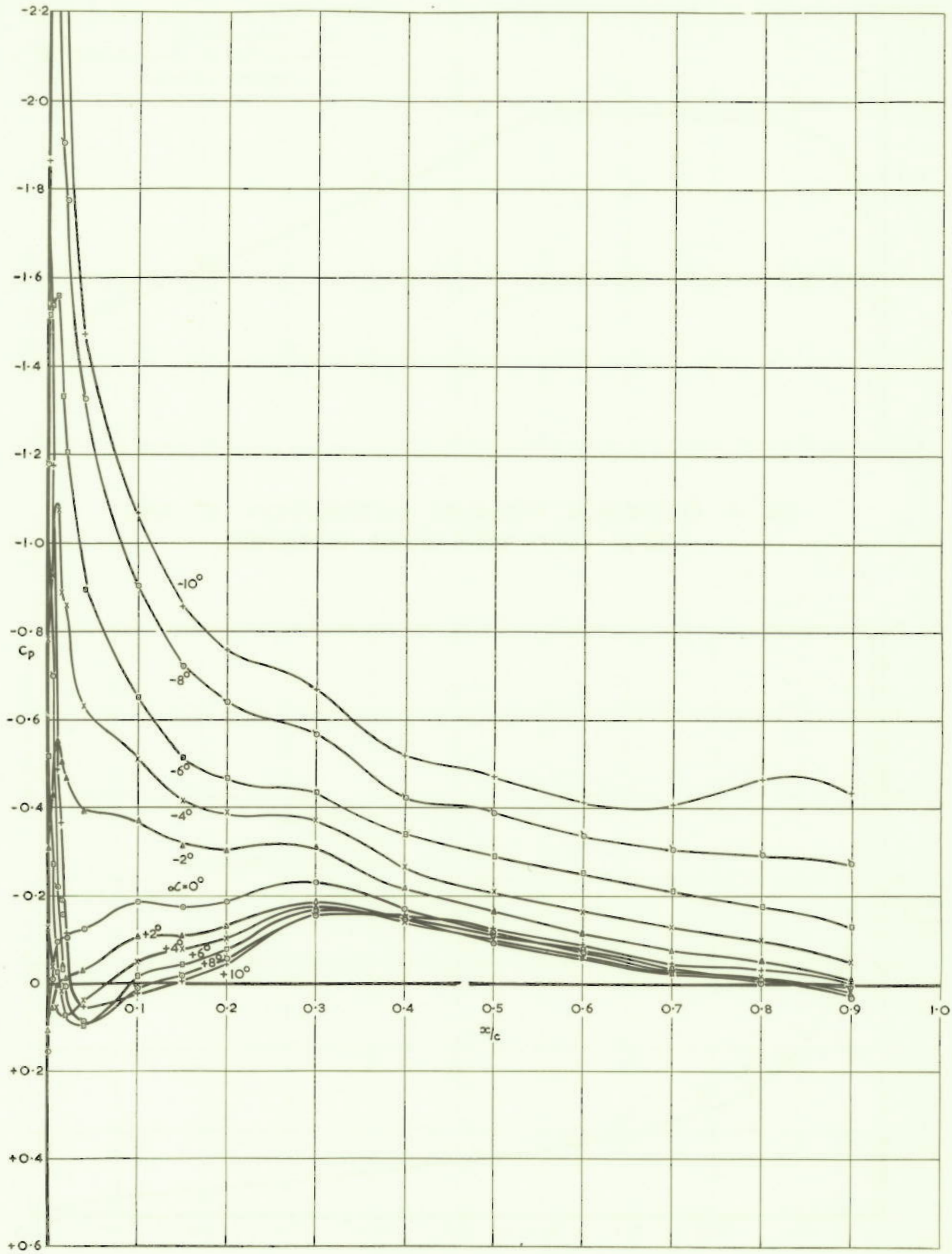

FIG. 3h. STATIC PRESSURE DISTRIBUTION FOR $R_e = 0{\cdot}88 \times 10^6 - 1{\cdot}86 \times 10^6$ PER FT.
STATION H – $\eta = 0 \cdot 9605$

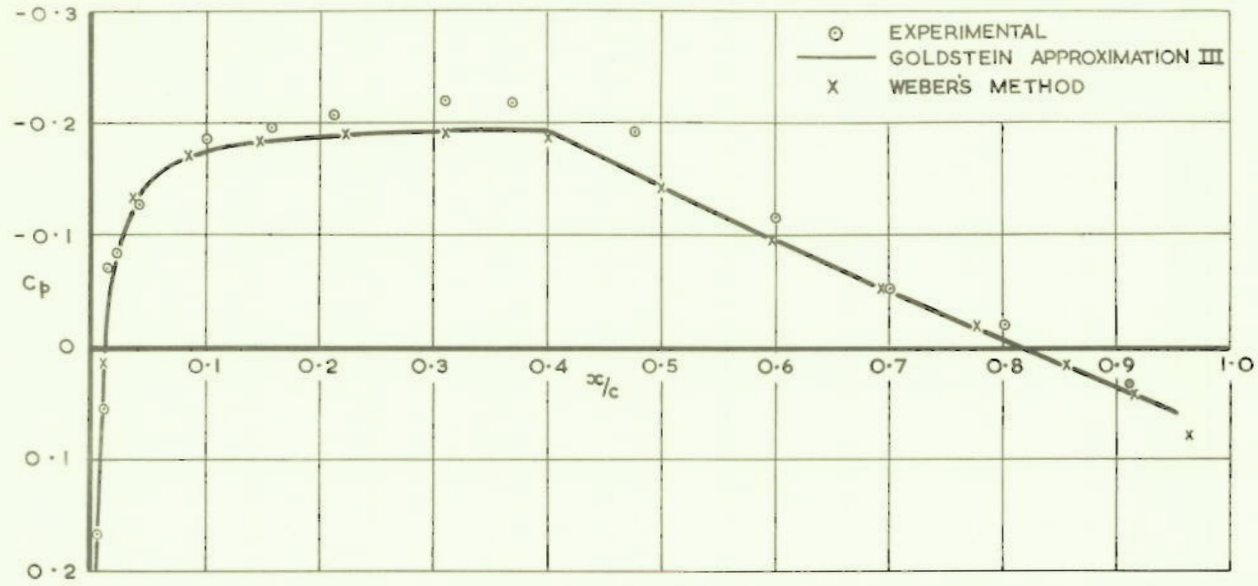

FIG. 4. CHORDWISE PRESSURE DISTRIBUTION AT MID SEMI-SPAN WITH ZERO INCIDENCE

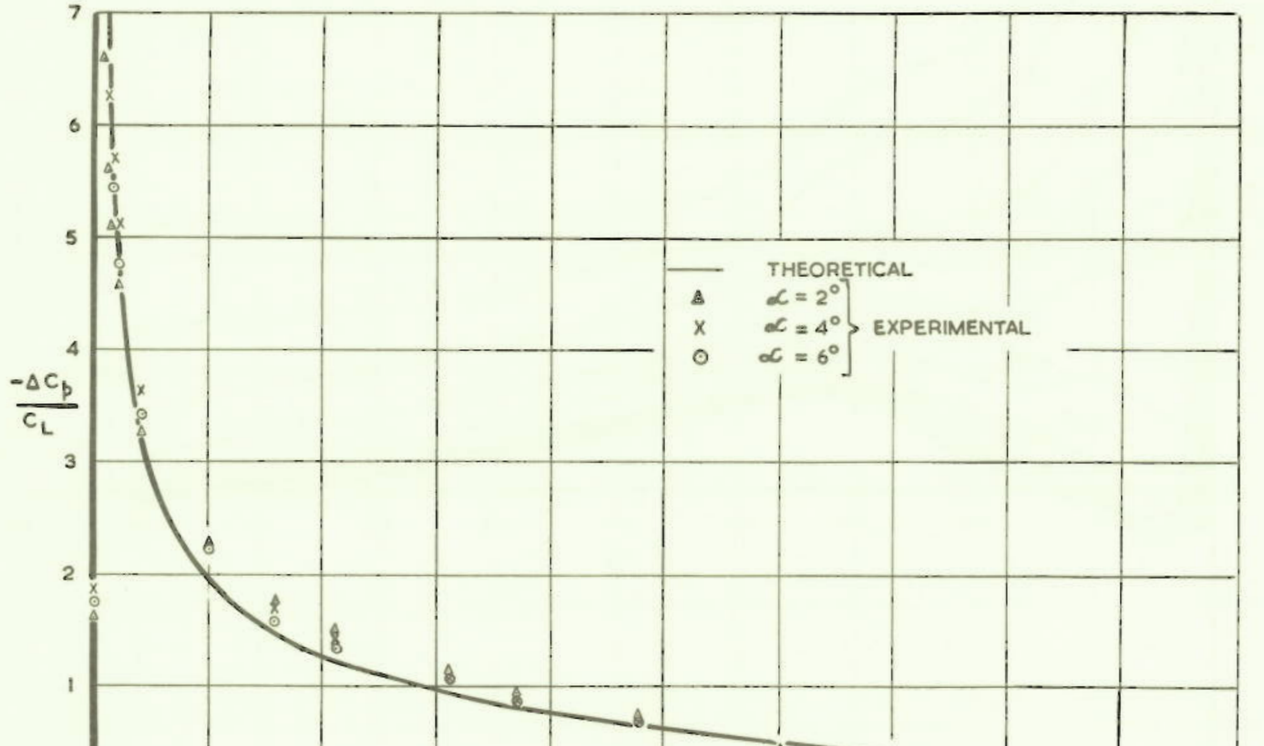

FIG. 5. CHORDWISE LOADING AT MID SEMI-SPAN

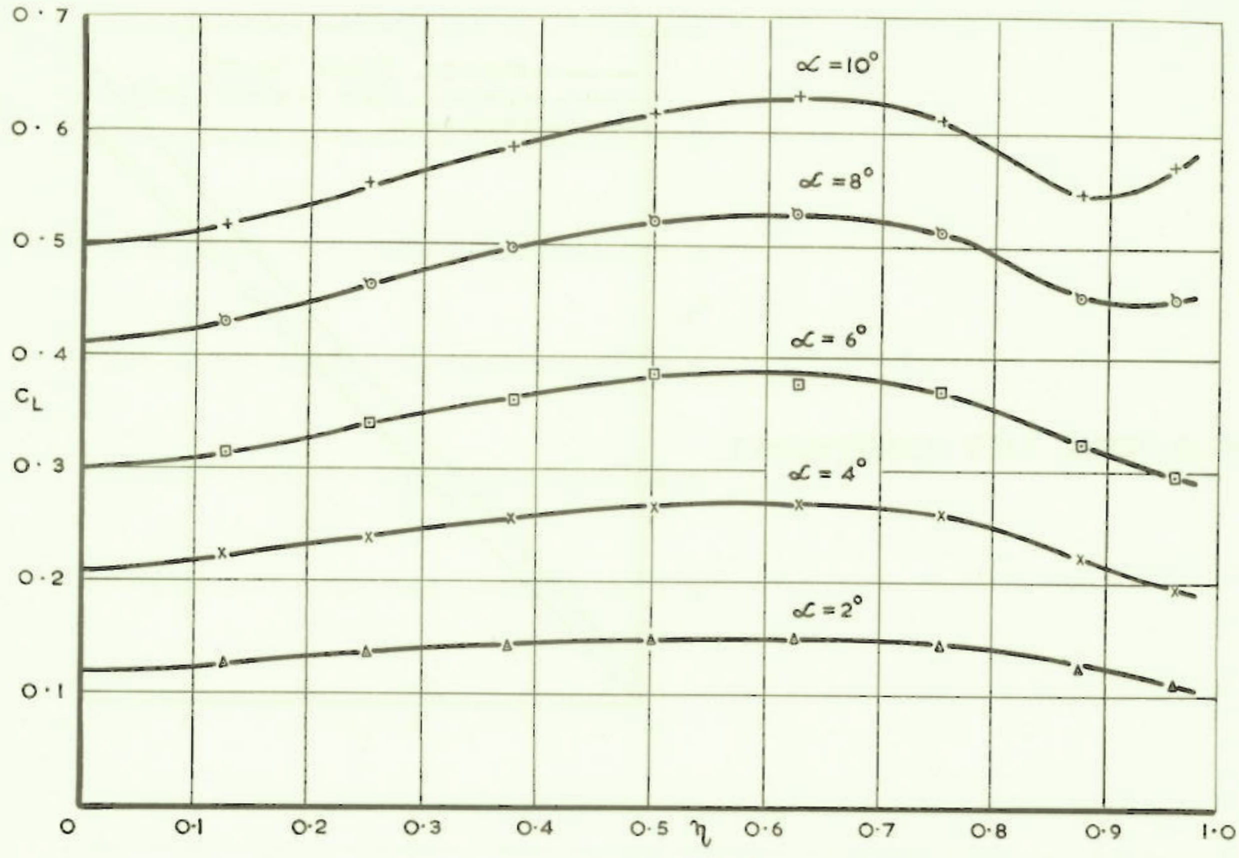

FIG. 6. DISTRIBUTION OF LOCAL LIFT COEFFICIENT.

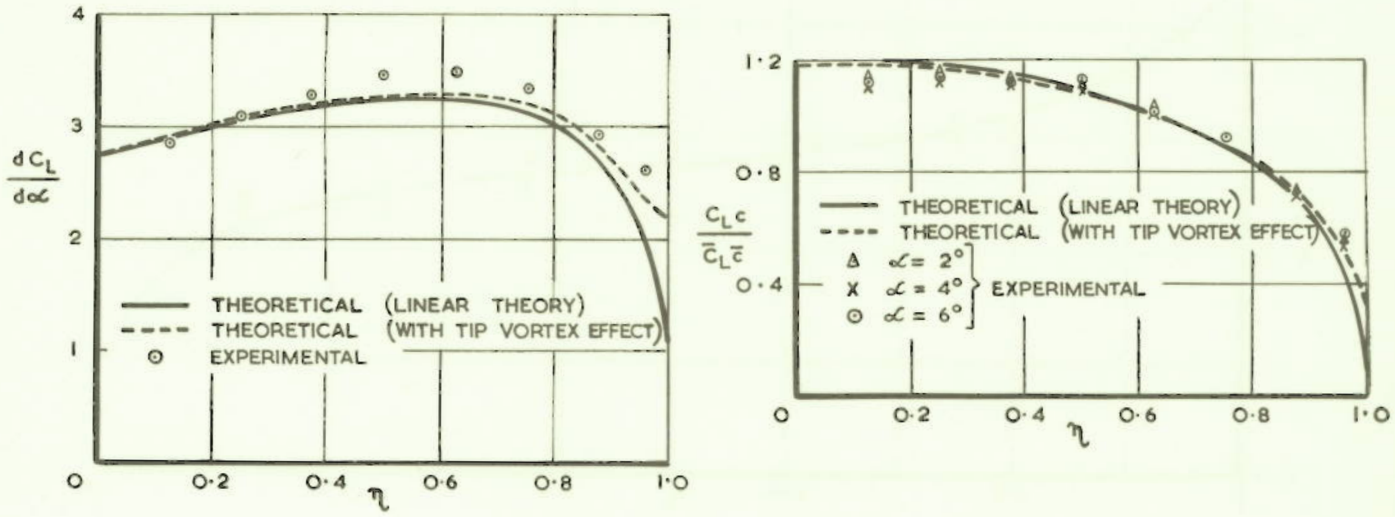

FIG. 7. MEASURED AND CALCULATED SPANWISE LOAD DISTRIBUTIONS.

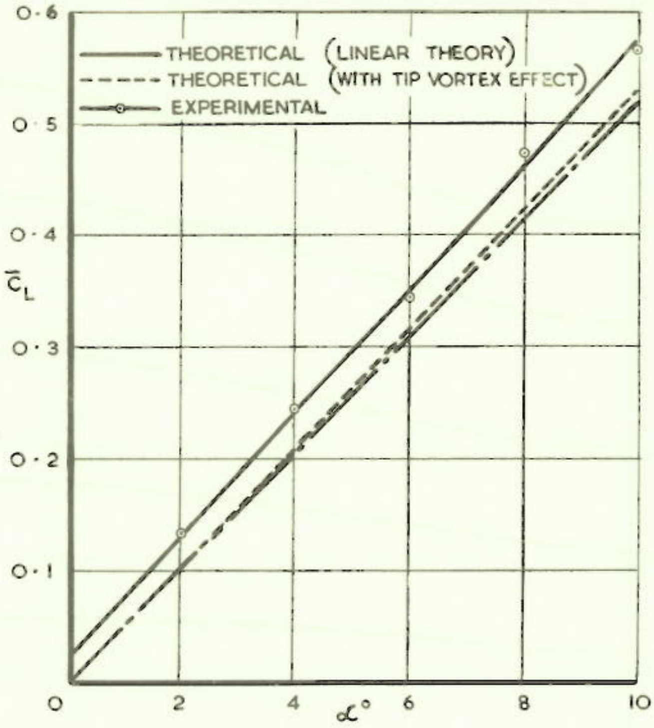

FIG. 8. TOTAL LIFT COEFFICIENT.

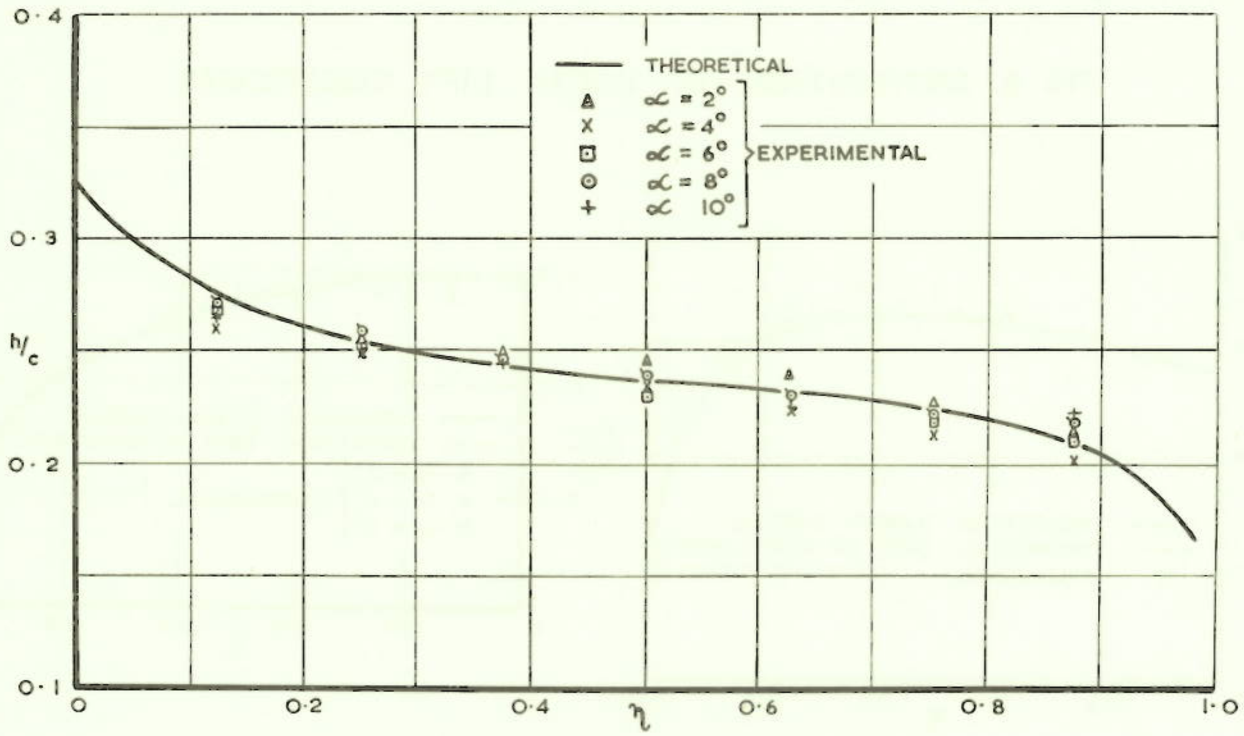

FIG. 9. POSITION OF LOCAL AERODYNAMIC CENTRE.

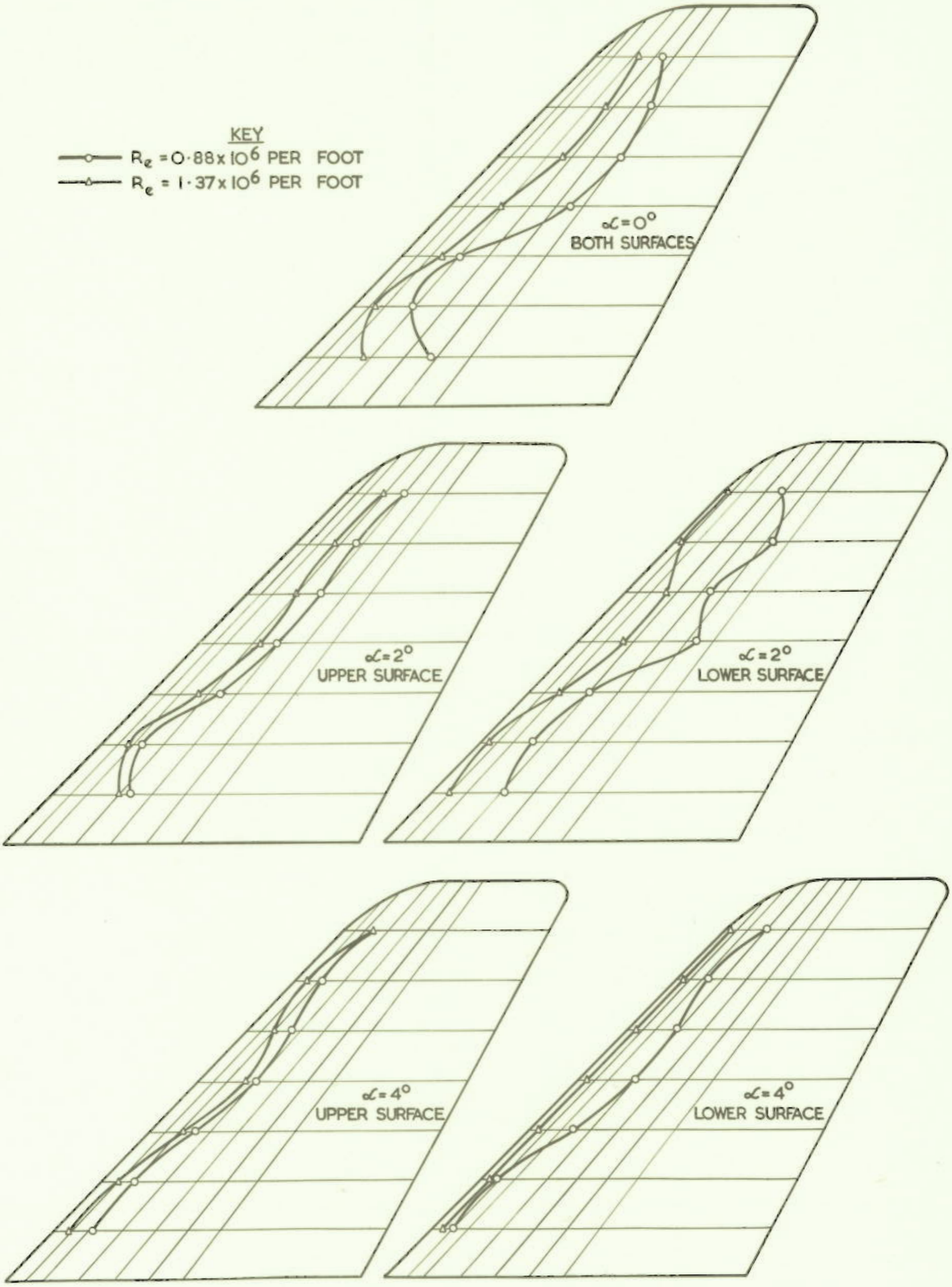

FIG. 10. LOCATION OF TRANSITION FRONTS.